IMMUNOLOGY

Pregnancy enhances antiviral immunity independent of type I IFN but dependent on IL-17–producing $\gamma\delta^+$ T cells in the nasal mucosa

Julia Chronopoulos[1,2], Erwan Pernet[2,3], Kim A. Tran[2,4], Toby K. McGovern[2], Arina Morozan[1,2], Sadie Wang[1,2], Oscar Tsai[2,5], Kosuke Makita[2], Maziar Divangahi[1,2,4,5]*†, James G. Martin[1,2]*†

Pregnancy is associated with profound changes in immunity. However, pregnancy-related respiratory immune adaptations in response to influenza infection and their impact on disease severity remain unclear. Here, we describe, in a preclinical model of mid-gestation pregnancy, a mechanism of enhanced host defense against influenza A virus (IAV) localized to the nasal cavity that limits viral replication and reduces the magnitude of intrapulmonary immune responses. Consequently, the pregnant mice show reduced pulmonary pathology and preserved airway function after IAV infection. The early restriction of viral replication is independent of type I interferon (IFN) but dependent on increased antimicrobial peptides (AMPs) driven by interleukin-17$^+$ (IL-17$^+$) $\gamma\delta^+$ T cells within the nasal passages. This pathway of host defense against IAV infection in the upper airways during pregnancy restricts early viral infection and prevents virus dissemination into the lung supporting maternal fitness.

INTRODUCTION

Influenza A virus (IAV) is among the deadliest threats to humanity, with pandemic strains emerging every few years (*1*). Pregnant women are reportedly at higher risk of developing severe disease during influenza outbreaks, specifically in their second and third trimesters (*2*), and is attributed to pregnancy resulting in an immunocompromised state required to tolerate a semi-allogeneic fetus (*3*). However, it is now well-established that pregnancy comprises transitional periods of distinct immunological states engaged at each trimester (*4*, *5*). The immune response during the major part of pregnancy is actively skewed toward type 2 immunity but is type 1 biased and proinflammatory in early pregnancy to allow for placentation and implantation and reverts to a proinflammatory state that promotes labor and placental rejection during the later stages of pregnancy (*3*). While much of the focus of the immunology of pregnancy pertains to the maternal-fetal interface, our understanding of immune responses driving maternal morbidity with infectious pathogens outside of this local environment is still incomplete.

Susceptibility to severe infection is not uniform across the population of pregnant women but rather may depend on individual immunity (*6*). A Canadian study reported that pregnant women experienced less severe outcomes compared to all H1N1 influenza–related cases during the 2009 pandemic, and only 1.5% of hospitalized pregnant women died (*7*), although a higher percentage (6%) has been reported in the United States (*8*). Emerging evidence from the recent COVID-19 pandemic further suggests that pregnant women experienced mild disease compared to the general population (*9*–*13*). Thus, host responses in pregnancy may be affected differently with different viral infections. Effective host defense against IAV is the result of an appropriate balance between host resistance, which is essential for reducing pathogen burden, and disease tolerance, which is crucial in limiting the extent of inflammation and subsequent tissue damage (*14*). Both aspects of host defense are required for effective immunity against pathogens (*15*). How host defense is affected by pregnancy is incompletely explored and, in particular, mechanisms of resistance that are likely present in some pregnant women.

Motivated by the adverse outcomes in a subset of IAV-infected pregnant women, most preclinical studies have focused on susceptibility to IAV infection during pregnancy using BALB/c mice, with a highly T helper 2 (T_H2) skewed immunity, which have shown that maternal morbidity in these mice is driven either by a lack of antiviral immunity (*16*) or exuberant inflammatory responses (*17*). Asthma- and non-asthma–related atopy have been linked to more severe infections with H1N1 (*18*, *19*). It is therefore expected that BALB/c mice manifest greater susceptibility to IAV infection. In contrast to the observations using BALB/c mice, IAV infection in pregnant C57BL/6 mice has revealed preserved airway function during IAV infection (*20*). However, the mechanism of the relative protection against airway dysfunction from IAV infection during pregnancy in the C57BL/6 mouse is unknown. In this study, we assessed the pulmonary response to IAV infection mid-gestation in C57BL/6 mice. We identified a mechanism of resistance that is dependent on enhanced immunity mediated by antimicrobial peptides (AMPs) within the nasal passages which require interleukin-17$^+$ (IL-17$^+$) $\gamma\delta^+$ T cells. Thus, in contrast to the current dogma suggesting that pregnancy increases host susceptibility to IAV infection, we have provided evidence that upper airway antimicrobial defenses limited pulmonary viral titers and promoted intrapulmonary disease tolerance.

RESULTS

Pregnancy enhances host resistance to IAV infection

First, we investigated disease severity by infecting nonpregnant and pregnant [embryonic day 10 (E10)] mice with a sublethal dose of IAV [A/Puerto Rico/8/34 H1N1 (PR8); 50 plaque-forming units (PFU)]

[1]Department of Medicine, McGill University, Montreal, Quebec, Canada. [2]Meakins-Christie Laboratories, Research Institute of the McGill University Health Centre, Montreal, Quebec, Canada. [3]Department of Medical Biology, Université du Québec à Trois-Rivières, Quebec, Canada. [4]Department of Pathology, McGill University, Montreal, Quebec, Canada. [5]Department of Microbiology and Immunology, McGill University, Montreal, Quebec, Canada.
*Corresponding author. Email: james.martin@mcgill.ca (J.G.M.); maziar.divangahi@mcgill.ca (M.D.)
†These authors contributed equally to this work.

intranasally (Fig. 1A) and monitored their morbidity through weight loss. The IAV-infected pregnant mice lost significantly less weight than the nonpregnant females compared to their respective uninfected controls (Fig. 1B). The pulmonary viral burden at 10 hours and day 1 (D1) post-IAV infection was significantly lower in pregnant mice compared to control groups (Fig. 1C). Using the reporter Ruby-NS1 PR8 strain (*21*), we examined the dissemination of IAV within the lungs and observed an overall reduction in infected cells in the airways (Fig. 1D) and parenchyma (fig. S1A) of the pregnant mice at day 3 postinfection. Since epidemiologically maternal morbidity worsens with gestational age (*2*), we asked whether maternal resistance in our IAV model persisted in the third trimester. IAV infection at E16 also resulted in reduced pulmonary viral titers in the pregnant mice (fig. S1B). Collectively, these data suggest that pregnancy in C57BL/6 mice afforded enhanced host resistance to IAV infection.

Assessment of the intrapulmonary inflammatory responses by flow cytometry showed that the frequency and absolute numbers of neutrophils and inflammatory monocytes were significantly reduced in the pregnant IAV-infected mice (Fig. 1, E and F, and fig. S1, D and E). Similarly, the levels of pulmonary inflammatory cytokines and chemokines [C-C motif chemokine ligand 2 (CCL2), keratinocyte-derived chemokine (KC), IL-6, and IL-1β] were significantly decreased, while the levels of anti-inflammatory IL-10 were increased in the pregnant IAV-infected mice (Fig. 1G-K). Therefore, the enhanced host resistance during pregnancy was not due to increased pulmonary proinflammatory responses.

Pregnancy limits IAV-induced immunopathology and preserves airway mechanics

One of the hallmarks of IAV replication is the induction of epithelial cell death (*22*). In agreement with the reduction in total viral burden, there were fewer infected epithelial cells (Fig. 2A) and cleaved/activated caspase-3^+ cells in the pregnant IAV-infected mice (Fig. 2, B and C). Consistent with reduced cell death in the intrapulmonary airways, bronchoalveolar lavage (BAL) fluid revealed decreased lactate dehydrogenase (LDH) in the pregnant IAV-infected mice (Fig. 2D). Also consistent with these findings, histology exhibited reduced areas of inflammation by 9 days post-IAV infection in the pregnant mice (Fig. 2E). Therefore, early control of viral replication in the pregnant mice was associated with reduced morbidity, pulmonary inflammation, cell death, and immunopathology.

IAV infection is associated with asthma attacks (*23*) and increases airway hyperresponsiveness (AHR) in a murine model of asthma (*24*). Thus, we next examined the consequences of IAV infection for airway dysfunction at days 0, 1, and 3 postinfection. IAV infection resulted in AHR to inhaled methacholine (MCh) by day 3 after infection concomitant with histological evidence of peribronchial and perivascular inflammation. In accordance with lower viral titers and a reduction in the subsequent parenchymal inflammation, these surrogates for virally induced acute asthma exacerbations were also significantly reduced in the pregnant mice at days 1 (Fig. 2F) and 3 (Fig. 2G) postinfection as determined by lower MCh-induced changes in respiratory resistance and elastance. This reduction in viral load and associated preservation of airway function were also not unique to syngeneic pregnancies as allogeneic pregnant females also had reduced pulmonary viral burden (fig. S1T) and lower AHR (fig. S1U) at day 3 postinfection compared to nonpregnant mice. Therefore, increased host resistance during pregnancy in C57BL/6 mice promotes disease tolerance in the airways and alveolar compartments of the lung minimizing pulmonary dysfunction.

Maternal resistance is independent of enhanced pulmonary antiviral immunity

Since the early control of viral replication is often orchestrated by the temporal production of interferons (IFNs) (*15*, *25*), we investigated their role in the protection of the lungs in IAV-infected pregnant mice. When quantifying type I (IFN-α/β) and III (IFN-λ) IFNs in lung homogenates, the concentrations of all three IFNs were significantly reduced in the pregnant IAV-infected mice (Fig. 3, A and B, and fig. S3A). To further support that the increased host resistance of the pregnant mice against IAV was type I IFN independent, we next used *Ifnar1*$^{-/-}$ mice. At day 3 post-IAV infection, although the total viral burden in both pregnant and nonpregnant *Ifnar1*$^{-/-}$ mice exceeded that of wild-type (WT) mice, pregnant mice showed an early resistance to IAV infection (at day 1 postinfection) (Figs. 1C and 3C). These data further confirmed that resistance attributable to pregnancy during very early stages of infection is independent of type I IFN-mediated antiviral immunity.

The protective role of alveolar macrophages (AMs) in IAV infection has been well documented, and their depletion quickly accelerates viral replication and renders the host highly susceptible to secondary bacterial infection and severe disease (*26*–*30*). Three days after IAV infection, although there were no differences in the frequency of AMs (Fig. 3D), the total number of AMs in the pregnant mice was significantly higher than controls (Fig. 3E). The increased number of AMs in the pregnant IAV-infected mice was associated with reduced apoptosis (caspase-3^+) (Fig. 3F) and not associated with increased in situ proliferation (Ki67$^+$) of AMs (fig. S3B). AMs adopt specific functional phenotypes along the inflammatory (M1) to regulatory (M2) spectrum by undergoing changes in surface marker expression, cytokine secretion, and metabolism in response to environmental stimuli and pulmonary pathogens (*31*). The observed susceptibility in BALB/c mice has been in part attributed to a more alternatively activated macrophage phenotype (*17*, *32*). Since our study modeled resistance, we investigated the possibility of a more "classical" functional AM phenotype in C57BL/6 pregnant mice. However, there were no differences in the frequency nor in mean fluorescence intensity (MFI) of arginase 1 (Arg1$^+$; M2 marker) or inducible nitric oxide synthase (iNOS$^+$; M1 marker) AMs between nonpregnant and pregnant mice (fig. S3C).

To further explore a possible AM adaptation favorable to pathogen elimination, we assessed their cellular metabolism in vitro by isolating AMs from the BAL fluid of nonpregnant and pregnant mice, infecting them with IAV [multiplicity of infection (MOI) of 1], and then subjecting them to Seahorse assay. AMs from pregnant mice did not show any evidence of enhanced glycolytic capacity (Fig. 3G) but had lower basal respiration before and following IAV infection (Fig. 3H) as well as lower maximal respiratory capacity at baseline (fig. S3F). These data suggest that AMs from pregnant mice do not adopt a specific functional program tailored toward antiviral immunity and proinflammatory effector functions.

We next investigated further whether the intrinsic properties of AMs from pregnant mice were responsible for host resistance to IAV infection. However, AMs isolated from the BAL fluid of naïve nonpregnant and pregnant mice infected in vitro with IAV (MOI of 1)

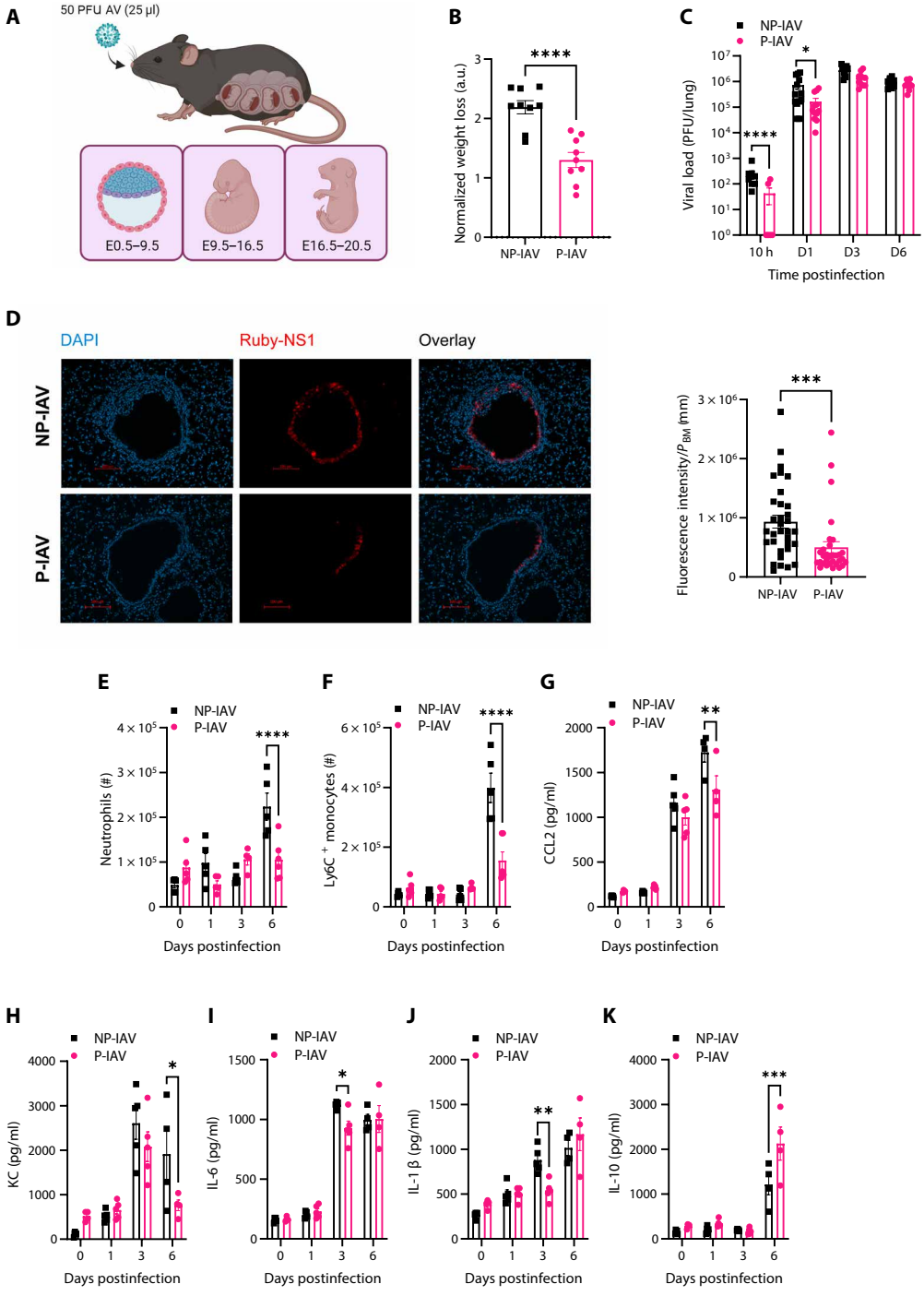

Fig. 1. Mid-gestation pregnancy provides enhanced host resistance to IAV infection. (**A**) Graphical representation of the experimental model. Created with BioRender.com. Nonpregnant (NP) and pregnant (P) (E10; second trimester-equivalent) C57BL/6 mice were infected intranasally with a sublethal dose of the PR8 strain of IAV (25 or 50 PFU). (**B**) Body weight was monitored daily for 12 days postinfection and is depicted as the difference between the area under the curves of weight over time for uninfected and infected mice. Body weight of infected mice was normalized to their respective uninfected controls ($n = 8$ to 9). a.u., arbitrary units. (**C**) Kinetics of the viral load measured by MDCK plaque assay on lung homogenates ($n = 6$ to 13). (**D**) Fluorescence microscopy of infected airways in the lungs of nonpregnant and pregnant mice 3 days after intranasal infection with a sublethal dose of the reporter Ruby-NS1 PR8 strain (500 PFU in 25 µl of PBS; $n = 4$ to 5). Scale bars, 100 µm. P_{BM}-airway basement membrane perimeter. DAPI, 4′,6-diamidino-2-phenylindole. (**E**) Neutrophil and (**F**) Ly6C$^+$ monocyte absolute numbers measured in lung homogenates of nonpregnant and pregnant IAV-infected mice by flow cytometry at various times postinfection ($n = 4$ to 6). (**G** to **K**) Pulmonary CCL2, KC, IL-6, IL-1β, and IL-10 concentrations of nonpregnant and pregnant IAV-infected mice measured by enzyme-linked immunosorbent assay (ELISA) at various time points postinfection ($n = 4$ to 5). Data are presented as mean ± SEM. with $^*P < 0.05$, $^{**}P < 0.01$, $^{***}P < 0.001$, and $^{****}P < 0.0001$. Data were analyzed using unpaired Student's *t* test (B), Mann-Whitney *U* test (D), or two-way analysis of variance (ANOVA) followed by Sidak's multiple comparisons test [(C) and (E) to (K)].

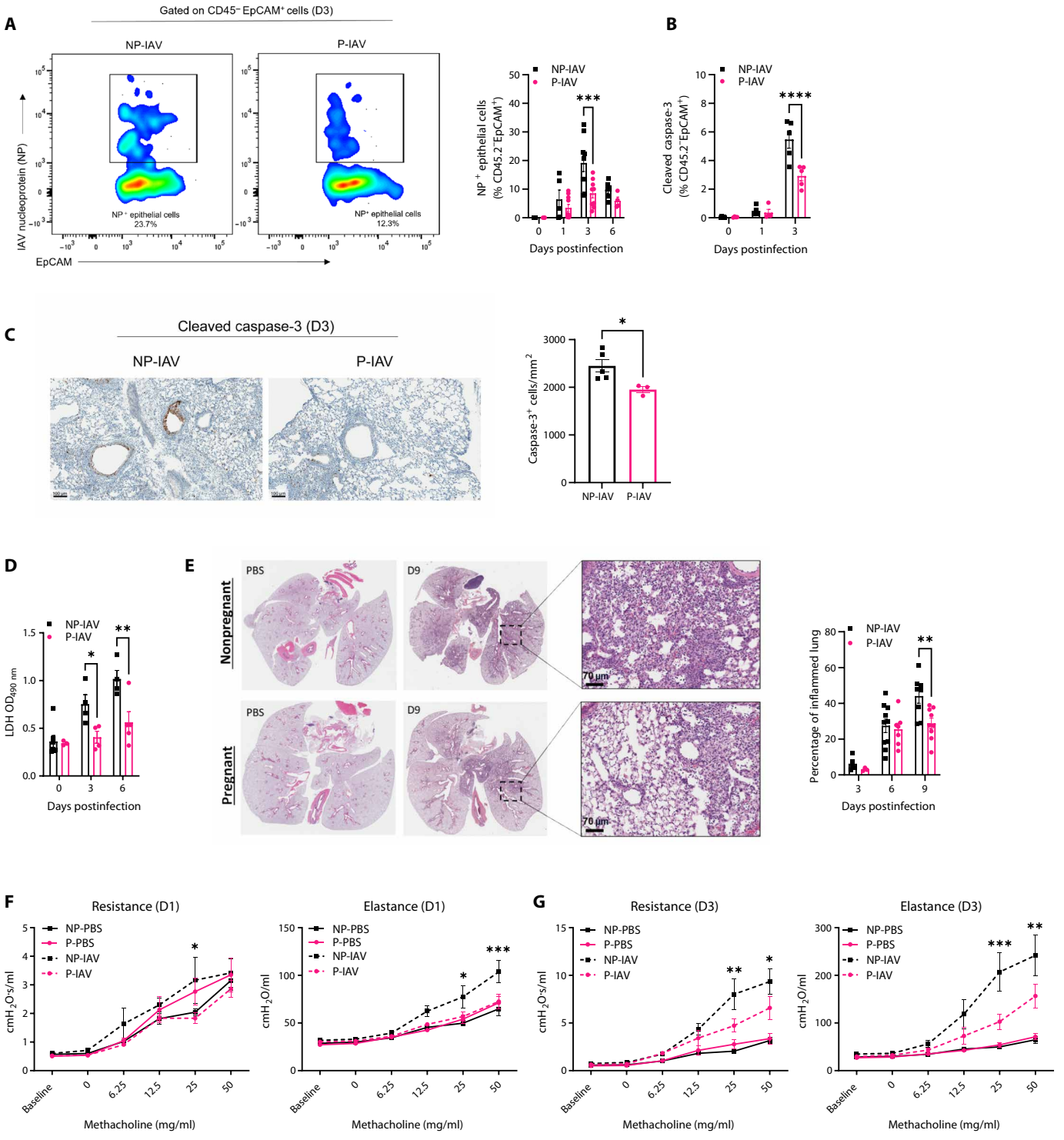

Fig. 2. Enhanced maternal host resistance limits IAV-induced pulmonary pathology and AHR. (**A**) Representative fluorescence-activated cell sorting (FACS) plots and quantification of infected lung epithelial cells gated on single, live, CD45.2$^-$EpCAM$^+$NP$^+$ (50 PFU; $n = 4$ to 10). NP, nucleoprotein of IAV. (**B**) Frequency of caspase-3$^+$ epithelial cells (CD45$^-$EpCAM$^+$Casp3$^+$) in the lungs of nonpregnant and pregnant mice at various times post-IAV infection (50 PFU; $n = 4$ to 5). (**C**) Immunohistochemical images from lung sections 3 days post-IAV infection stained with anti–caspase-3 and the respective quantification (50 PFU; $n = 3$ to 5). Scale bars, 100 µm. (**D**) Kinetics of LDH released in BAL fluid of nonpregnant and pregnant mice at various time points post-IAV infection (50 PFU; $n = 3$ to 7). OD_{490}, optical density at 490 nm. (**E**) Representative lung photomicrographs and quantification from nonpregnant and pregnant naïve and IAV-infected mice at various days postinfection stained with hematoxylin and eosin (50 PFU; $n = 3$ to 10). Scale bars, 70 µm. Respiratory mechanics measured on days (**F**) 1 and (**G**) 3 post-IAV infection using flexiVent following challenge with increasing doses of methacholine (MCh; 50 PFU; $n = 4$ to 10). Data are presented as mean ± SEM. with $^*P < 0.05$, $^{**}P < 0.01$, $^{***}P < 0.001$, and $^{****}P < 0.0001$. Data were analyzed using two-way ANOVA followed by Sidak's multiple comparisons test [(A), (B), (D), and (E)] or Tukey's multiple comparisons test [(F) and (G)] or unpaired Student's *t* test (C).

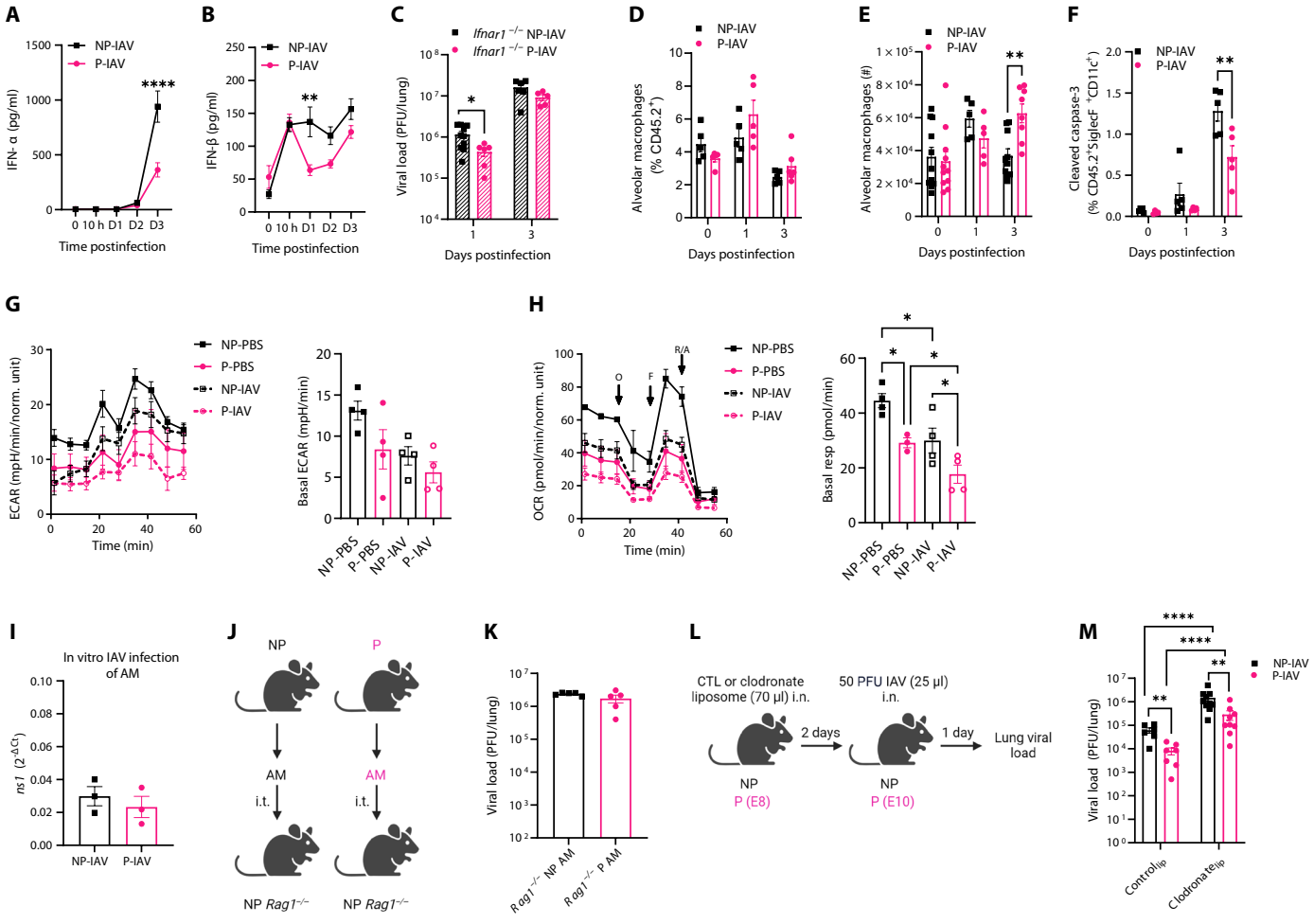

Fig. 3. Resistance to IAV infection is independent of pulmonary type I IFN-mediated antiviral immunity and AMs. Kinetics of (**A**) IFN-α and (**B**) IFN-β concentrations measured in lung homogenates by ELISA (50 PFU; $n = 3$ to 5). (**C**) Kinetics of pulmonary viral load in *Ifnar1*$^{-/-}$ mice measured by MDCK plaque assay (50 PFU; $n = 5$ to 10). (**D**) AM frequency and (**E**) absolute numbers measured in lung homogenates by flow cytometry (50 PFU; $n = 5$ to 11). (**F**) Frequency of pulmonary apoptotic AMs (CD45.2$^+$SiglecF$^+$CD11c$^+$Casp3$^+$) at various time points post-IAV infection (50 PFU; $n = 4$ to 5). (**G**) Extracellular acidification rate (ECAR) and (**H**) oxygen consumption rate (OCR) of AMs by Seahorse assay before and after 24 hours of infection with HIN1 (MOI of 1) ($n = 8$ to 10 mice pooled and plated in replicates). O, oligomycin; F, fluorocarbonyl cyanide phenylhydrazone; R/A, antimycin A/rotenone. (**I**) Naïve AMs derived from the BAL fluid of nonpregnant and pregnant mice infected in vitro with IAV (MOI of 1) for 24 hours and viral *Ns1* expression quantified by RT-qPCR ($n = 8$ to 10 mice pooled and plated in triplicates). (**J**) Naïve AMs from the BAL fluid of nonpregnant and pregnant mice adoptively transferred intratracheally (i.t.) (5×10^4 cells per 50 µl) into *Rag1*$^{-/-}$ recipient mice and infected intranasally (i.n.) 2 hours posttransfer (50 PFU IAV). Created with BioRender.com. (**K**) Pulmonary viral load of *Rag1*$^{-/-}$ recipient mice 3 days postinfection by MDCK plaque assay ($n = 5$). (**L**) Murine AM depletion via intranasal administration of 70 µl of control (CTL) or clodronate liposome 2 days before IAV infection (50 PFU). Created with BioRender.com. (**M**) Pulmonary viral load 1 day post-IAV infection measured by MDCK plaque assay following AM depletion ($n = 6$ to 10). Data are presented as mean ± SEM. with $^*P < 0.05$, $^{**}P < 0.01$, and $^{****}P < 0.0001$. Data were analyzed using two-way ANOVA followed by Sidak's multiple comparison [(A) to (F) and (M)], one-way ANOVA followed by Holm- Šidák's multiple comparisons test [(G) and (H)], or unpaired Student's *t* test [(I) and (K)].

had comparable viral replication [nonstructural protein 1 (Ns1) expression] after a 24-hour infection (Fig. 3I). These data were supported by adoptively transferring AMs derived from nonpregnant and pregnant mice into nonpregnant *Rag1*$^{-/-}$ mice, which were then infected with IAV (50 PFU) (Fig. 3J). There was no difference in the control of viral replication among AM transferred groups on day 3, which was the peak of IAV replication (Fig. 3K). To further confirm that AMs did not account for the protection against IAV during pregnancy, AMs were depleted via intranasal administration of clodronate liposomes as previously described (*30*), which resulted in ~80% depletion (fig. S3I). Pulmonary viral titers were then quantified 1 day post-IAV infection at the onset of differences in host resistance between nonpregnant and pregnant mice (Fig. 3L). As expected, the total viral burden in both groups increased following AM depletion, confirming the important role of AMs in restricting viral replication (*29*, *33*). However, the AM depletion did not abrogate the relative protection in the pregnant mice (Fig. 3M). Therefore, although canonically known for their indispensable role in antiviral immunity, AMs were not responsible for the enhanced resistance during pregnancy.

IL-17A$^+$ γδ$^+$ T cells restrict IAV replication in the upper airways during pregnancy

Given that pulmonary antiviral mechanisms were not responsible for maternal resistance against IAV, we hypothesized that the lower airways were not as easily accessible to IAV in the pregnant mice, suggesting that antiviral immunity may be initiated in the upper

airways. To test this hypothesis, we bypassed the upper airways by infecting the pregnant mice via the intratracheal route (50 PFU IAV in 50 μl) (Fig. 4A) and found that the protection in the pregnant IAV-infected mice was completely abrogated (Fig. 4B). These data indicate that the ability of pregnant mice to restrict viral replication is mainly mediated by upper respiratory tract antiviral immunity.

To investigate further whether the upper airways can restrict IAV replication during pregnancy, we harvested nasal cavity tissue from nonpregnant and pregnant mice after IAV infection, and we assessed viral load by plaque assay (Fig. 4C). Viral replication was significantly reduced in the pregnant IAV-infected mice at days 1 and 3 postinfection (Fig. 4D). To determine the location of viral restriction in the upper airways, we used the Ruby-NS1 PR8 strain and observed a marked reduction in the intensity and number of infected nasal epithelial cells, specifically in the olfactory region of the nasal mucosa (zone III) in the pregnant mice (Fig. 4E). It has been previously reported in pregnant rats that maternal morbidity is attributable to an increase in sialoglycan receptors facilitating viral entry (*34*). To investigate whether the reduction in nasal viral burden was a consequence of reduced viral attachment, we assessed the nasal cavity of naïve mice for the IAV receptors, α2,3- and α2,6-sialic acids, using *Maackia amurensis* and *Sambucus nigra* agglutinin lectins, respectively, by flow cytometry. However, there were no significant differences in the frequency (fig. S4B) nor MFI (fig. S4C) of sialic acid receptors between nonpregnant and pregnant mice. Unexpectedly, this resistance in the nasal cavity was also independent of type I IFN-mediated antiviral immunity as pregnant *Ifnar1*$^{-/-}$ mice had lower viral titers at day 1 postinfection compared to nonpregnant controls (Fig. 4F).

Considering that type I IFNs did not account for the protection at the early stage of infection, we shifted our focus to IL-17, an important cytokine produced at mucosal surfaces reported to provide host resistance to IAV infection during the early phases of infection (*35*). The expression levels of *il-17A* by reverse transcription quantitative polymerase chain reaction (RT-qPCR) were significantly up-regulated in the pregnant mice at days 1 and 3 post-IAV infection compared to nonpregnant mice (Fig. 4G). It has been previously shown that pulmonary γδ$^+$ T cells are the dominant IL-17–producing cells following IAV infection (*36*). Therefore, we isolated cells from the nasal cavities of naïve and 1-day post–IAV-infected nonpregnant and pregnant mice and stimulated them with murine recombinant IL-1β (rIL-1β) and recombinant IL-23 (rIL-23) (*37*). Naïve pregnant mice had a higher proportion of γδ$^+$ T cells isolated from the nasal cavities (Fig. 4H) and a higher absolute cell count 1-day post-IAV infection (Fig. 4I). During pregnancy, γδ$^+$ T cells accounted for ~65% of all IL-17A–producing cells (Fig. 4J), and following IAV infection, the pregnant mice had higher IL-17A$^+$γδ$^+$ T cell counts compared to nonpregnant mice (Fig. 4K). There was no significant difference in IL-17A production by either CD4$^+$ T cells (fig. S4H) or CD3$^-$RORγT$^+$ cells (fig. S4I) between nonpregnant and pregnant mice. Moreover, pregnant *TCR*δ$^{-/-}$ mice had less nasal *il-17A* expression than their WT counterparts (fig. S4K) and similar levels to nonpregnant *TCR*δ$^{-/-}$ mice (fig. S4L). Compared to WT, pregnant *TCR*δ$^{-/-}$ mice also exhibited higher nasal *Ns1* and matrix protein 1 (M1) expression (Fig. 4, L and M) similar to the levels observed in nonpregnant WT and *TCR*δ$^{-/-}$ mice (Fig. 4, N and O, and fig. S4, M to O). These results indicate that nasal IL-17A–expressing γδ$^+$ T cells are increased during pregnancy, and a lack of these cells leads to less effective control of viral replication in pregnant mice.

IL-17A induces antimicrobial immunity in the upper airways to restrict IAV replication during pregnancy

Early IL-17 secretion has been shown to induce bacterial clearance in the upper and lower airways via AMP production (*38*, *39*). Furthermore, IL-17$^+$γδ$^+$ T cells have been implicated in restricting IAV replication in the trachea (*35*) and lungs (*40*, *41*) during early infection, and AMP secretion during early IAV infection is an important primary innate host defense mechanism (*42*). AMPs such as cathelicidins [LL37; mouse ortholog cathelicidin-related antimicrobial peptide (CRAMP)], defensins [e.g., mouse β-defensin (mBD)], and mucins (MUC) interfere with viral pathogenesis by direct inhibition of virus-host interactions, destabilizing viral envelopes, and reducing viral replication and host immunomodulation (*42*–*46*). The respiratory region (zone II) is the main site of mucin and AMP synthesis in the nasal mucosa (*47*). Considering this, we also found an up-regulation of multiple AMPs including *Muc5ac*, *Cramp*, *Mbd-3*, *Mbd-4*, and *Mbd-14* (Fig. 5, A to E) in the pregnant IAV-infected mice that largely mimicked the kinetics of *il-17A* expression. Principal components analysis (PCA) identified *Ns1* and AMP expression as key contributors in distinguishing between the groups. Specifically, *Ns1* was primarily found in the nonpregnant group (PC1 < 0), while AMP expression was predominantly localized within the pregnant group (PC1 > 0) (Fig. 5F and fig. S5D). Furthermore, although all AMPs were negatively associated with viral replication, *Cramp* and *Mbd-3* were significantly inversely correlated at the peak of viral replication (Fig. 5F). To determine the link between IL-17 and AMP production, we neutralized IL-17 (anti–IL-17A antibody) (Fig. 5G) and found that the expression levels of AMPs in the pregnant IAV-infected mice were either reduced to values similar to or below nonpregnant mice (Fig. 5, H to K). This reduction in AMP production resulted in comparable nasal viral replication between nonpregnant and pregnant mice (Fig. 5L).

The protective effects of IL-17 against infectious pathogens are often accompanied by an influx of neutrophils (*35*, *39*, *48*). Furthermore, AMPs can promote chemotaxis of leukocytes, predominantly of neutrophils and monocytes/macrophages, to aid in viral and bacterial clearance (*35*, *39*, *49*, *50*). Similarly, we found that the pregnant mice had a significantly greater number of neutrophils, monocytes, and macrophages in the nasal cavities 1 day post-IAV infection (Fig. 5, M to O). Therefore, we propose that the immune protection during pregnancy is mediated via two distinguished programs: the early phase, which leads to increased induction of IL-17A$^+$γδ$^+$ T cells and the production of AMPs which limits the initial viral replication in the upper airways, and the late phase which subsequently modulates innate immune responses to maintain viral restriction through type I IFN signaling in the lower airways.

To investigate whether this protection could be recapitulated in nonpregnant mice, we administered recombinant IL-17A (rIL-17A) intranasally before IAV infection (fig. S5H). Although IL-17A increased *Muc5ac* expression (fig. S5I), both groups had comparable nasal *Cramp*, *Mbd-3*, *Mbd-4*, and *Ns1* expression (fig. S5, J to M). Therefore, it seems that this IL-17–AMP axis mediating upper airway resistance to IAV is specific to pregnancy in that additional pregnancy-related factors appear to be needed to invoke protection. However, recombinant mBD-3 (rmBD-3) exhibited direct antiviral effects when preincubated with IAV before infection of murine

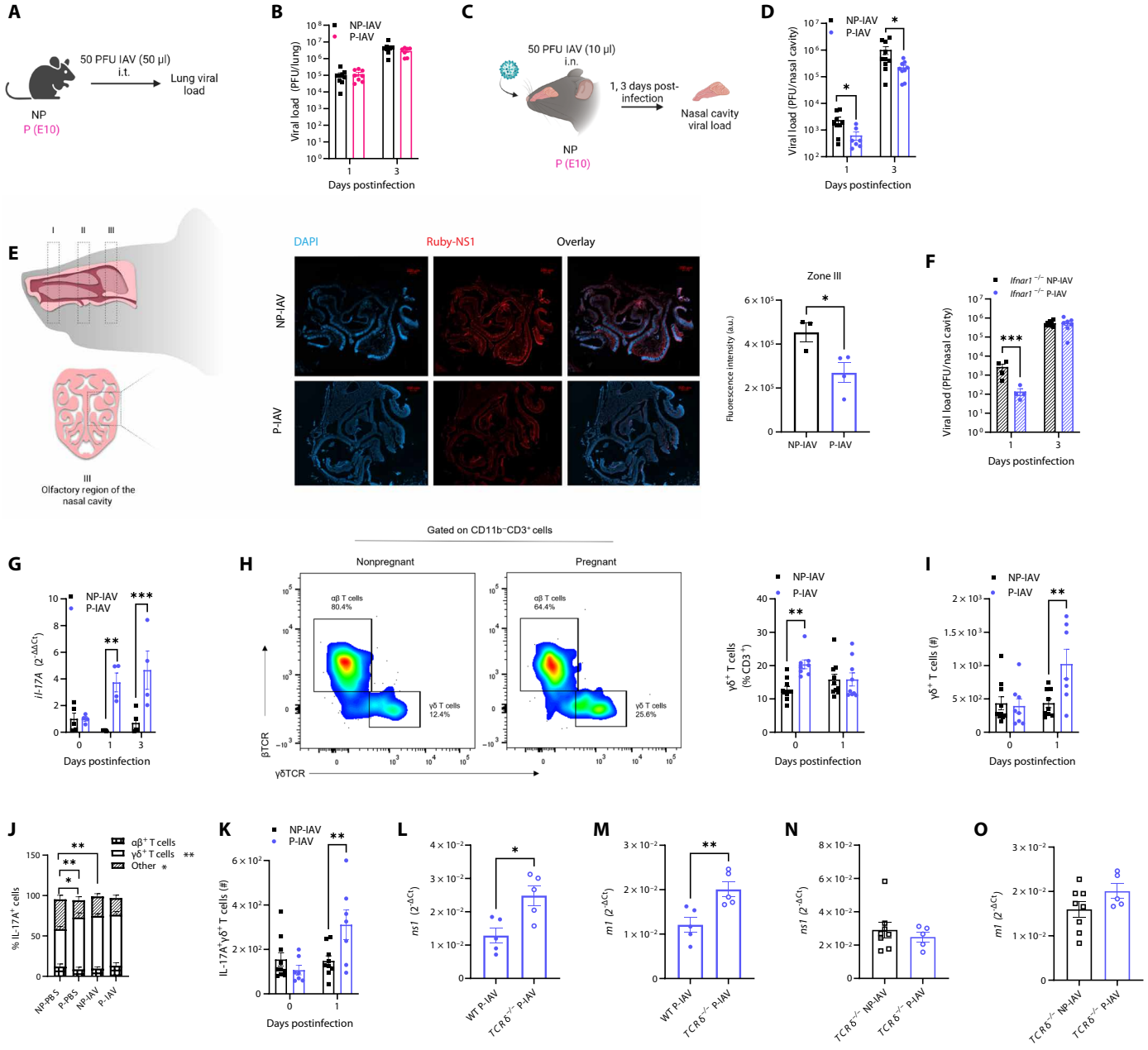

Fig. 4. IL-17A$^+$ γδ$^+$ T cells restrict IAV replication in the nasal cavities of pregnant mice. (**A**) Model of murine intratracheal IAV infection (50 PFU in 50 µl of PBS). Created with BioRender.com. (**B**) Kinetics of pulmonary viral titers by MDCK plaque assay following intratracheal IAV infection ($n = 7$ to 9). (**C**) Graphical representation of upper airway infection (50 PFU IAV in 10 µl of PBS). Created with BioRender.com. (**D**) Kinetics of the viral load measured by MDCK plaque assay on nasal tissues from WT nonpregnant and pregnant mice ($n = 7$ to 10). (**E**) Graphical representation of nasal tissue regions and fluorescence microscopy of infected olfactory epithelial cells (zone III) with quantification 3 days postinfection with Ruby-NS1 PR8 (500 PFU in 10 µl of PBS) ($n = 3$ to 4). Scale bars, 200 µm. (**F**) Kinetics of viral load measured by MDCK plaque assay on nasal tissues of nonpregnant and pregnant *Ifnar1*$^{-/-}$ mice (50 PFU; $n = 4$ to 7). (**G**) Kinetics of nasal *il-17A* expression by RT-qPCR (50 PFU; $n = 4$ to 5). (**H**) Representative FACS plots and frequency of γδ$^+$ T cells, (**I**) absolute number of γδ$^+$ T cells, (**J**) proportion of IL-17A–producing cells and (**K**) total number of IL-17A$^+$γδ$^+$ T cells in nasal tissues of nonpregnant and pregnant mice at 0 and 1 day post-IAV infection following 4 hours of stimulation with rIL-23 (10 ng/ml) and rIL-1β (10 ng/ml) (50 PFU; $n = 7$ to 10). (**L**) *Ns1* and (**M**) *M1* expression in nasal tissues of WT and *TCR*δ$^{-/-}$ pregnant mice by RT-qPCR 3 days post-IAV infection (50 PFU; $n = 5$). (**N**) *Ns1* and (**O**) *M1* expression in nasal cavities of *TCR*δ$^{-/-}$ nonpregnant and pregnant mice 3 days post-IAV infection ($n = 5$ to 8). Data produced from Fig. 4 (L) and (M). Data are presented as mean ± SEM. with $^*P < 0.05$, $^{**}P < 0.01$, and $^{***}P < 0.001$. Data were analyzed using two-way ANOVA followed by Sidak's multiple comparisons [(B), (D), and (F) to (K)], unpaired Student's *t* test [(E), (L), (N), and (O)], or Mann-Whitney *U* test (M).

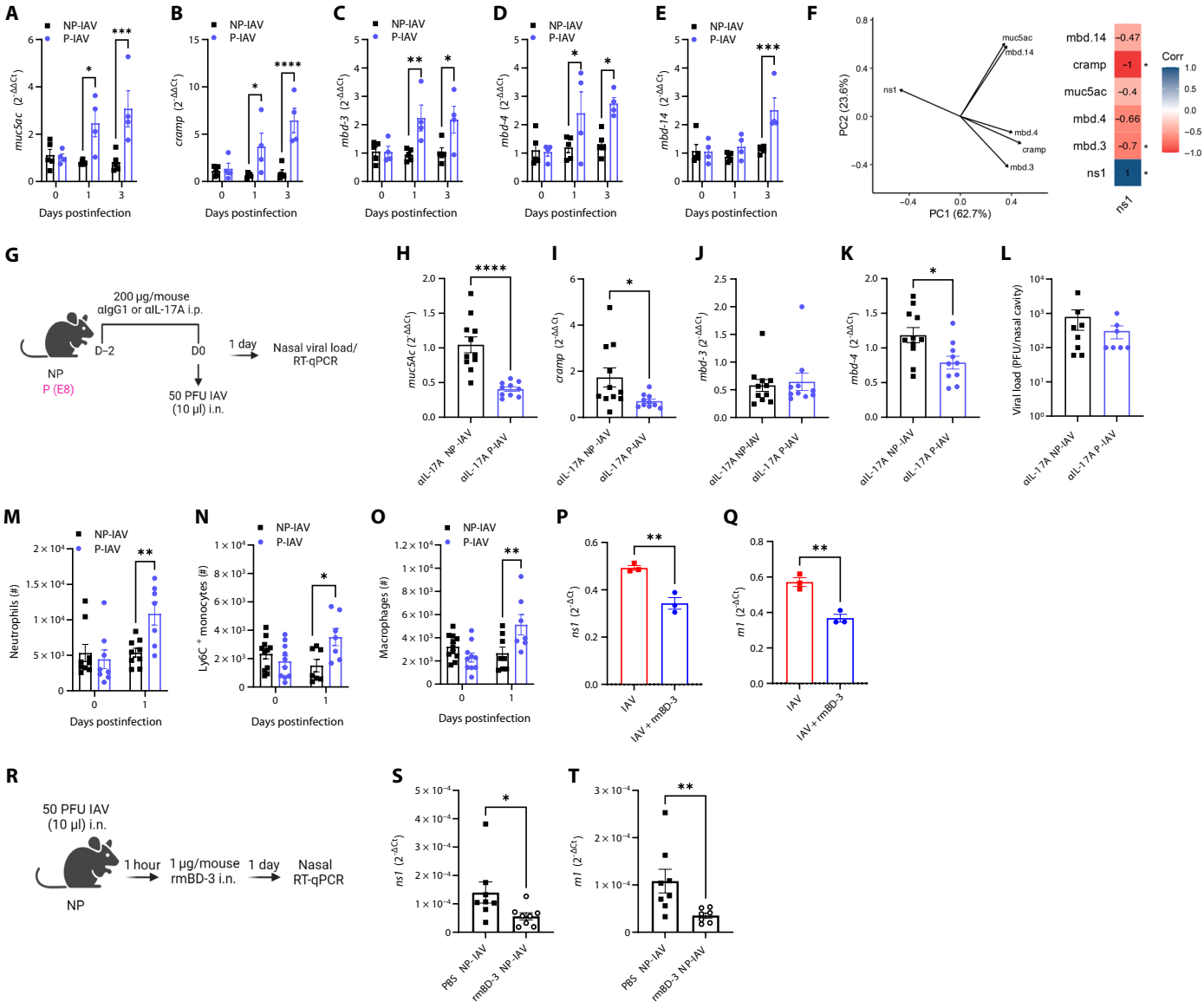

Fig. 5. Antimicrobial immunity restricts IAV replication in the upper airways. (**A** to **E**) *Muc5ac*, *Cramp*, *Mbd-3*, *Mbd-4*, and *Mbd-14*, expression in the nasal cavities of nonpregnant and pregnant IAV-infected mice measured by RT-qPCR at various time points postinfection (50 PFU; $n = 4$ to 5). (**F**) Loading plot and correlation coefficients of *Ns1* and AMP expression by RT-qPCR 3 days post-IAV infection ($n = 4$ to 5). (**G**) Intraperitoneal (i.p.) administration of anti-IgG1 (αIgG1) or anti–IL-17A (αIL-17A) (200 µg per mouse in 200 µl of PBS) to nonpregnant and pregnant mice 2 days before and the day of IAV infection (50 PFU in 10 µl). Created with BioRender.com. (**H** to **K**) Quantification of nasal *Muc5ac*, *Cramp*, *Mbd-3*, and *Mbd-4* expression by RT-qPCR ($n = 10$ to 11) and (**L**) nasal viral titers quantified by MDCK plaque assay 1 day post-IAV infection following intraperitoneal administration of αIL-17A ($n = 7$ to 8). (**M** to **O**) Neutrophil, monocyte, and macrophage absolute numbers in the nasal cavities of nonpregnant and pregnant mice at days 0 and 1 post-IAV infection measured by flow cytometry (50 PFU; $n = 7$ to 11). Viral (**P**) *Ns1* and (**Q**) *M1* gene expression measured by RT-qPCR in murine epithelial cells 24 hours post-IAV infection (MOI of 1) with/without recombinant mBD-3 (rmBD-3; 100 µg/ml) ($n = 3$). (**R**) Intranasal administration of rmBD-3 (1 µg per mouse; in 10 µl PBS) 1 hour post-IAV infection (50 PFU in 10 µl of PBS) to nonpregnant mice. Created with BioRender.com. Viral (**S**) *Ns1* and (**T**) *M1* gene expression measured by RT-qPCR in nasal tissues of nonpregnant mice 1 day post-IAV infection with/without rmBD-3 ($n = 7$ to 8). Data are presented as mean ± SEM. with $^*P < 0.05$, $^{**}P < 0.01$, $^{***}P < 0.001$, and $^{****}P < 0.0001$. Data were analyzed using two-way ANOVA followed by Sidak's multiple comparisons [(A) to (E) and (M) to (O)], Pearson's correlation (F), unpaired Student's *t* test [(H), (K), (L), (P), and (Q)], or Mann-Whitney *U* test [(I), (J), (S), and (T)].

epithelial cells (Fig. 5, P and Q), and when administered in vivo following IAV infection (Fig. 5R), it reduced nasal viral replication 24 hours after infection (Fig. 5, S and T). Therefore, although IL-17 alone may not be sufficient outside of the context pregnancy to reduce viral replication, AMPs exhibit significant antiviral capacity in the upper airways.

DISCUSSION

Pregnant women are faced with contradictory demands to maintain immune tolerance required for fetal survival versus mounting an appropriate immune response to invading pathogens (*51*). However, the consequences of pregnancy-associated immune changes on outcomes of infection beyond the maternal-fetal interface are still

unclear. Many of the immune changes occurring during pregnancy and their impact on host defense have often been explored in BALB/c mice and in allogeneic pregnancies which model well the subset of women who develop severe disease following IAV infection who are highly T_H2 biased, which is also an excellent model for a small fraction of pregnant women with severe susceptibility to IAV infection (*5*, *16*, *17*, *32*). However, this does not represent the vast majority of IAV infection in pregnant women who do not develop severe disease requiring hospitalization. Thus, in the current study, we have investigated the site within the respiratory tract of host resistance mechanisms against IAV infection during pregnancy.

Here, we showed pregnant C57BL/6 mice infected with IAV revealed enhanced host defense against infection, specifically via augmented antiviral immunity in the nasal passages. The reduced viral replication in the nasal cavities of the pregnant mice resulted in significant reduction in viral propagation within the lungs with subsequent decreased pulmonary inflammation, immunopathology, and airway dysfunction, the latter of which has been previously demonstrated by Vermillion *et al.* (*20*). Therefore, the increased host resistance promotes disease tolerance in both the airways and alveolar compartments of the lung. Whereas this strain-dependent protection is reportedly attenuated in allogeneic pregnancy when C57BL/6 females are crossed with BALB/c males (*5*, *52*), our data indicated that host resistance and preservation of lung function were equally conserved during allogeneic pregnancy. This study introduces a pregnancy model of resistance inherent in the C57BL/6 mice which can be harnessed to further our understanding of pregnancy-related immune adaptations and their influence on host defense. Furthermore, our findings conceptually highlight the interplay between host resistance in upper versus lower airways whereby the initial pathogen load reduced the magnitude of the immune response and consequently its associated collateral tissue damage to maintain lung function.

The resistance of pregnant C57BL/6 mice to IAV infection is in sharp contrast to the observed susceptibility manifested by BALB/c mice, which is in part attributed to a more alternatively activated macrophage phenotype (*17*, *32*). However, in our study, AMs from pregnant mice did not adapt their metabolism nor their phenotype in a manner that would promote viral clearance. Neither AMs from nonpregnant nor pregnant mice adopted a shift toward glycolysis following IAV infection. Moreover, neither their depletion nor their adoptive transfer abrogated the relative differences in viral load between nonpregnant and pregnant mice. Whereas IAV quickly depletes AMs and significantly compromises host defenses and increases morbidity and mortality (*26*, *29*, *53*), in our study, the AM population was conserved during pregnancy as a consequence of reduced cell death. This finding is likely attributable to a reduction in viral burden in the lower airways.

Pregnancy-induced adaptations of the upper respiratory tract include increased mucopolysaccharides in the naso- and oropharyngeal mucosa which in ~18 to 30% of patients result in nasal congestion (*54*–*56*). While the etiology of this gestational rhinitis is unknown, it may act as a host defense strategy against respiratory infections as it has been shown in other mucosal barriers. For instance, AMPs and mucus secreted in cervico-vaginal fluid and uterine tissues are essential primary barriers to invading pathogens (*57*–*61*), and their expression changes throughout the menstrual cycle and pregnancy (*62*). The assessment of IL-17A expression by nasal immune cells by flow cytometry suggested that $\gamma\delta^+$ T cells were a significant source. Nasal $CD4^+$ T cells and $CD3^-ROR\gamma T^+$ cells did not significantly respond to in vitro stimulation with rIL-1β and rIL-23, although these cells isolated from the intestine showed substantial responses. Although these experiments do not definitively exclude these cells as possible contributors to IL-17A production in vivo, the absence of $\gamma\delta^+$ T cells impaired the restriction of viral replication and reduced *il-17A* expression in pregnant mice. Analogously, uterine $\gamma\delta^+$ T cells, are the major source of IL-17 within the female reproductive tract (*61*, *63*, *64*) and provide protection against viral (*61*, *65*, *66*), fungal (*67*), and bacterial infections (*68*).

Several limitations of the study warrant consideration. Although epithelial cells are the predominant producers of β-defensins, macrophages and neutrophils have also been shown to secrete defensins and LL37/CRAMP (*49*, *69*–*71*). Therefore, future studies are necessary to elucidate the cellular source of AMPs within the nasal passages and whether they are directly interacting with IAV and restricting replication and/or are promoting chemotaxis of inflammatory cells to clear infection. In addition, other possible sources of IL-17, such as mucosal-associated invariant T cells, were not assessed. Furthermore, the absence of optimal effect on viral load or general AMP expression following rIL-17A administration to nonpregnant mice may not reflect an independence of the response to IAV infection but may relate to unfavorable bioavailability, pharmacodynamics, and timing of administration.

Considering that maternal fitness is essential for the survival of the fetus, pregnancy must evolutionarily adopt a different strategy of host defense against pulmonary pathogens. Augmenting upper airway antimicrobial immunity can be an adaptation for preserving lung function from increased viral replication and subsequently massive inflammatory responses and tissue damage. However, while we provide evidence of one pathway of maternal resistance, pregnancy is a complex state characterized by substantial immunological, physiological, and metabolic changes with considerable cross-talk between epithelial cells, immune cells, hormones, and the presence of a semi-allogeneic fetus. Although our study identifies one upper airway host defense mechanism against pulmonary IAV infection during pregnancy, it is unlikely that maternal host resistance solely relies on a single mechanism. Expanding our findings is essential to uncover additional factors contributing to maternal resistance against IAV infection. Continued research in this domain is critical to fully elucidate maternal resistance mechanisms that support maternal health.

MATERIALS AND METHODS

Mice

Eight- to 10-week-old female WT, *Rag1*$^{-/-}$ (B6.129S7-*Rag1*$^{tm1Mom/J}$), IFN-α/β receptor deficient (*Ifnar1*$^{-/-}$) (B6.129S2-*Ifnar1*^{tm1Agt}/Mmjax), and T cell receptor delta chain deficient (*TCR*δ$^{-/-}$) (B6.129P2-*Tcrd*^{tm1Mom}/J) C57BL/6 mice were purchased from the Jackson Laboratory housed, and bred with male C57BL/6 or BALB/c mice at the animal facility of the Research Institute of the McGill University Health Centre. All protocols were approved by the Animal Care Committee of McGill University (permit nos. 2010-5860 and 2021-8244) in accordance with the guidelines set out by the Canadian Council on Animal Care.

Infection

Pregnant mice were infected on day 10 postmating (E10) or E16 with the mouse-adapted influenza A/Puerto Rico/8/34 (H1N1) virus provided by J. A. McCullers (St. Jude Children's Research Hospital). The

Ruby-NS1 PR8 strain provided by N. Heaton (Duke University) was used for fluorescent imaging of infected cells in the lungs and nasal cavities. Virus was propagated and titrated in Madin-Darby Canine Kidney [MDCK; American Type Culture Collection (ATCC)] cells using standard plaque assays (*72*). Under light anesthesia with isoflurane, mice were intranasally or intratracheally infected with sublethal doses of 25 or 50 PFU (PR8) and 500 PFU (Ruby-NS1) in 25 or 50 μl of phosphate-buffered saline (PBS) for lung studies and 10 μl of PBS for nasal cavity studies.

Isolation of nasal tissues

Following euthanasia, the skin was removed to expose the skull. The head was dissected from the body, and the lower jaw and tongue were excised. The eyes, surrounding tissues, and zygomatic bones were then removed, and the skull was cut along a sagittal plane to expose the nasal cavities. Both halves of the nasal cavities were removed from the rest of the skull, and all associated tissues were scraped from the inner surfaces of the cavities.

Quantification of viral load

Viral titers were determined in lung homogenates and nasal cavities [in 500 μl of Dulbecco's Modified Eagle medium (DMEM)] using MDCK plaque assays or by RT-qPCR assessing the viral genes, *Ns1* and *M1*, using a GENEzol TriRNA Pure extraction kit (Geneaid). MDCK cells were plated in six-well plates at a density of 750, 000 cells per well in complete DMEM (Gibco), 10% fetal bovine serum (FBS) (heat-inactivated; Wisent), 1% 200 mM L-glutamine (Gibco), and 1% 100× antibiotic-antimycotic (Gibco), at 5% CO_2, 37°C. After 48 hours, the cell layer was washed two times with PBS and incubated with 100 μl of lung or nasal homogenates for 1 hour. The inoculum was washed once with PBS, and wells were topped with 2× MEM (Thermo Fisher Scientific) and 1% agarose (Sigma-Aldrich) in a 1:1 ratio supplemented with L-1-tosylamido-2-phenylethyl chloromethyl ketone (TPCK) trypsin (2 μl/ml; Gibco). Plates were inverted and incubated (5% CO_2, 37°C) for 48 hours. Cells were then fixed with methanol (Thermo Fisher Scientific) and acetic acid (glacial; Thermo Fisher Scientific) at a ratio of 3:1. The agarose plugs were removed, and plates were dried for 24 hours under the fume hood.

Assessment of morbidity

Nonpregnant and pregnant mice were administered PBS or 50 PFU IAV intranasally. Change in body weight was measured daily until pregnant mice gave birth (12 days). To account for the impact of pregnancy on morbidity, the change in body mass relative to gestational age-matched uninfected animals was analyzed. The body weight of each infected animal per group was normalized to their respective uninfected controls and plotted per day postinfection. The differences between the area under the curves generated from these data between control and infected mice were then used to compare nonpregnant and pregnant IAV-infected mice.

Fluorescence microscopy

Lungs were inflated with 1 ml of 4% paraformaldehyde (PFA) by intratracheal cannulation, excised from the thoracic cavity, and placed in 4% PFA overnight. Lungs were washed in PBS twice over 48 hours and transferred into a sucrose/optimal cutting temperature compound (OCT) (Tissue-Tek) solution overnight. Lungs were then placed in OCT-filled blocks and flash-frozen in liquid nitrogen. Blocks were cut in 5-μm sections using a cryostat (Leica Biosystems). For nasal cavities, skin was removed from the skull, and heads were placed in 4% PFA overnight and transferred to PBS for another 24 hours. Skulls were then serially transferred into 15 and 30% sucrose supplemented with 0.1% sodium azide over 2 days. Tissues were sectioned and mounted with anti-fade mounting medium with 4′,6-diamidino-2-phenylindole (Vector Laboratories). Images were quantified with ImageJ. For nasal images, background-corrected fluorescence intensity was calculated as integrated density − (area of selected cell × mean fluorescence of background readings) and expressed in arbitrary units (*73*).

Assessment of lung pathology

BAL fluid was collected with a 26-gauge needle through the tracheal cannula using 3 × 1 ml cold, sterile PBS. The total volume recovered after lavage was ~0.7 ml. Samples were centrifuged at 1500 rpm for 10 min. LDH in BAL fluid supernatants was quantified using a commercial assay (CytoTox 96 Non-Radioactive Cytotoxicity Assay, Promega), following the manufacturer's recommendations. In addition, lungs were perfused through the right ventricle with 10 ml of PBS and subsequently fixed in inflation with 1 ml of formalin instilled intratracheally. Lungs were immersed in 5 ml of 10% formalin for 48 hours and then placed in 10 ml of 70% ethanol before paraffin embedding. Sections were stained with hematoxylin and eosin. The extent of inflammation present in hematoxylin and eosin–stained lung tissue was quantified using the Aperio ImageScope (Leica Microsystems, USA). The percentage of inflammation expresses the ratio of the total inflamed area to the total lung area determined by manual digitization of areas infiltrated with inflammatory cells and the outer perimeter of the lung, respectively. Quantification was analyzed by an observer blinded to the group status. For the quantification of apoptotic cells, 4-μm-thick sections were deparaffinized, rehydrated, and incubated for 24 min at 37°C with anti–cleaved caspase-3 (1:300; #96615, Cell Signaling) and then incubated with secondary antibody OmniMap anti-rabbit horseradish peroxidase (#760-4311, Roche) for 20 min at room temperature followed by a ChromoMap DAB detection kit (#760-4304, Roche). Slides were then counterstained with hematoxylin, dehydrated, cleared, and cover-slipped. Slides were digitally scanned with Aperio Turbo 2T scanner for morphometric analysis with Imagescope software.

Cytokine and chemokine production

IFN-β and IFN-α concentrations in lung homogenates were quantified using the Verikine Mouse IFN-β enzyme-linked immunosorbent assay (ELISA) kit (PBL Assay) or Mouse IFN-β ELISA kit (Abcam) and Verikine Mouse IFN-α ELISA kit (PBL Assay). IFN-λ, IL-6, IL-1β, CCL2, and KC were quantified by ELISA in lung homogenates according to the manufacturer's instructions (R&D Systems).

Flow cytometry–immunophenotyping

Lung tissues were perfused through the vasculature with 10 ml of PBS, harvested, minced, and digested with collagenase type I (Worthington CLS-1; 150 U ml^{-1}), deoxyribonuclease I (Worthington D; 1000 U ml^{-1}), and elastase (Worthington ESL; 80 U ml^{-1}) for 30 min at 37°C. Nasal cavities were harvested as previously described (*74*) and subjected to the same enzymatic digestion. Enzymes were neutralized with 300 μl of heat-inactivated FBS, lung and nasal digests were sieved through a 70- or 100-μm nylon mesh, and red blood cells were lysed with ammonium-chloride-potassium lysing buffer. Lung and nasal samples were resuspended, cell counts were determined with a hemacytometer, and ~1,000,000 cells were used for staining.

Cells were initially stained with the eBiosciences fixable viability dye eFluor 506 (Invitrogen, catalog no. 65-0863-18) or eFluor 780 (Thermo Fisher Scientific, catalog no. 65-0865-14) for 30 min at 4°C in PBS and anti-CD16/32 (BD Biosciences; clone 2.4G2) in 1% bovine serum albumin (BSA)/PBS solution to block nonspecific interaction with Fc receptors (10 min; 4°C). To identify innate immune cells and epithelial cells, cells were surface-stained (30 min; 4°C) with BV786-conjugated or phycoerythrin (PE)–conjugated anti-SiglecF (BD Biosciences; clone E50-2440); BUV737-conjugated or BUV395-conjugated anti-CD45.2 (BD Biosciences; clone 104); BUV395-conjugated anti-CD11b (BD Biosciences; clone M1/70); peridinin chlorophyll (PerCP)-eFluor710–conjugated anti-Ly6G (BD Biosciences; clone 1A8); allophycocyanin (APC)–conjugated or fluorescein isothiocyanate (FITC)–conjugated anti-Ly6C (BD Biosciences; clone AL-21); PE-Cy7–conjugated, BV786-conjugated, or BV421-conjugated anti-CD11c (BD Biosciences; clone HL3); PeCy7-conjugated anti-MerTK (Thermo Fisher Scientific; clone DS5MMER); PE-conjugated (Thermo Fisher Scientific; clone X54-5/7.1) or PerCP-Cy5.5–conjugated (BioLegend; clone X54-5/7.1) anti-CD64; APC-conjugated anti-F4/80 (Thermo Fisher Scientific; clone BM8); BV650-conjugated anti-NK1.1 (BD Biosciences; clone PK136); and APC-conjugated anti-CD326 (EpCAM) (BD Biosciences; clone G8.8).

To identify adaptive immune cells, cells were surface-stained with PerCP-conjugated (BioLegend; clone 30-F11) or FITC-conjugated (BD Biosciences; clone 104) anti-CD45.2, BV711-conjugated anti-CD138 (BioLegend; clone 281-2), BUV395-conjugated (BD Biosciences; clone ID3) or BV421-conjugated anti-CD19 (BD Biosciences; 6D5), PerCP-eFluor710–conjugated anti-gamma delta TCR (Thermo Fisher Scientific; clone GL3), FITC-conjugated (BioLegend; clone 17A2) or PE-conjugated anti-CD3 (Thermo Fisher Scientific; clone 145-2C11), BV510-conjugated (BioLegend; clone RM4-5) or V450-conjugated anti-CD4 (Thermo Fisher Scientific; clone GK1.5), and Alexa Fluor 700–conjugated anti-CD8a (BD Biosciences; clone 53-6.7).

For intracellular staining, cells were fixed and permeabilized using BD CytoFix/CytoPerm (BD Biosciences, catalog no. 554714) and stained with APC-conjugated anti-Ki67 (Thermo Fisher Scientific; clone SolA15), APC-conjugated anti-iNOS (Thermo Fisher Scientific; clone CXNFT), PeCy7-conjugated anti-Arg1 (Thermo Fisher Scientific; clone A1exF5), PE-conjugated anti-caspase-3 (BD Biosciences; clone C92-605), and FITC-conjugated anti-IAV nucleoprotein (Abcam, catalog no. ab20343; clone AA5H).

To assess the expression of NeuAc(α2-3)Gal and NeuAc(α2-6)Gal receptors in the nasal cavity, cells were stained with BUV737-conjugated anti-CD45.2, PE-conjugated anti-CD326 (EpCAM) (BD Biosciences; clone G8.8), biotinylated *M. amurensis* (Vector Laboratories, Burlingame, CA; catalog no. B-1315-2), Cy5-conjugated *S. nigra* agglutinin (Vector Laboratories, Burlingame, CA; catalog no. CL-1305-1), and PeCy7-conjugated streptavidin (BioLegend, catalog no. 405206) (30 min; 4°C).

Cytokine stimulation

For the characterization of IL-17A synthesis within the nasal passages, 500,000 nasal cells were plated in a 24-well plate in 1 ml of stimulation medium [RPMI (Gibco), 10% FBS (heat-inactivated; Wisent), 1% 200 mM L-glutamine (Gibco), 1% of 100× antibiotic-antimycotic (Gibco), and 0.1% β-mercaptoethanol (Gibco)], stimulated with rIL-23 (10 ng/ml) (BioLegend, catalog no. 589004) and rIL-1β (10 ng/ml) (BioLegend, catalog no. 575104) and incubated with GolgiStop (1:1000) (BD Biosciences, catalog no. 554724) for 4 hours at 5% CO_2, 37°C. Cells were then surface-stained with fixable viability dye eFluor 506, BUV737-conjugated anti-CD45.2, BV650-conjugated anti-CD3 (BioLegend; clone 145-2C11), APC-eFluor780–conjugated anti-TCR beta (Thermo Fisher Scientific; clone H57-597), and FITC-conjugated anti-TCR gamma/delta (BioLegend; clone GL3) (30 min; 4°C). Cells were then permeabilized using the Foxp3/Transcription Factor Staining Buffer Set (Thermo Fisher Scientific, catalog no. 00-5523-00) and intracellularly stained with Alexa Fluor 647–conjugated anti–IL-17A (BioLegend; clone TC11-18H10.1) and BV786-conjugated RORγT (BD Biosciences; clone Q31-378) (50 min; 4°C). Flow cytometry was performed on the BD LSRFortessa X-20 (BD Biosciences) using FACSDiva Software version 8.0.1 (BD Biosciences). Analysis was performed using FlowJo software version 10.10.

RNA isolation and RT-qPCR

RNA was extracted from nasal cavities using the GENEzol TriRNA Pure extraction kit (Geneaid). RNA was reverse-transcribed using the LunaScript RT SuperMix kit (New England Biolabs), as directed by the manufacturer, and cDNA was quantified using BrightGreen SYBR Green (Applied Biological Materials) by qPCR. Cq values of all target genes including *Gapdh* (forward, 5′-GGTCCTCAGTGTAGCC CAAG-3′; reverse, 5′-AATGTGTCCGTCGTGGATCT-3), *Ns1* (forward, 5′-AGAAAGTGGCAGGCCCTCTTTGTA-3′; reverse, 5′-TGTCCTG-GAAGAGAAGGCAATGGT-3′), *M1* (forward, 5′-TCAGGCCCCCT-CAAAGCCGA-3′;reverse, 5′-GGGCACGGTGAGCGTGAACA-3′), *Muc5ac* (forward, 5′-CCATGCAGAGTCCTCAGAACAA-3′; reverse, 5′-TTACTGGAAAGGCCCAAGCA-3′), *Mbd-1* (forward, 5′-CCAGATGGAGCCAGGTGTTG-3′; reverse, 5′-AG CTGGAGCG-GAGGACAAATG-3′), *Mbd-2* (forward, 5′-AAGTATTGGATAC-GAAGCAG-3′; reverse, 5′-TGGCAGAAGGAGGACAAATG-3′), *Mbd-3* (forward, 5′-GCATTGGCAACACTCGTCAGA-3′; reverse, 5′-CGGGATCTTGGTCTTCTCTA-3′), *Mbd-4* (forward, 5′-GCAGC-CTTTACCCAAATTATC-3′; reverse, 5′-ACAATTGCCAATCTGTC-GAA-3′),*Mbd-14* (forward,5′-GTATTCCTCATCTTGTTCTTGG-3′; reverse, 5′-AAGTACAGCACACCGGCCAC-3′), surfactant protein d (forward, 5′-TGTGATGGTGGGAATGGGTCAGAA-3′; reverse, 5′-TGTGGTGCCAGATCTTCTCCATGT-3′), *Cramp* (forward, 5′-AAGGAACAGGGGGTGGTG-3′; reverse, 5′-CCGGGAAAT-TTTCTTGAACC-3′), *il-17A* (forward, 5′-CACCTCACACGAG-GCACAAG-3′; reverse, 5′-GCAGCAACAGCATCAGAGACA-3′), *il-22* (forward, 5′-TTCCAGCAGCCATACATCGTC-3′; reverse, 5′-TCGGAACAGTTTCTCCCCG-3′), and *ifn*-γ (forward, 5′-ATGAACGCTACACACTGCATC-3′; reverse, 5′-CCATCCTTTT-GCCAGTTCCTC-3′) were obtained on a CFX96 PCR System (Bio-Rad) and analyzed using the formula either $2^{-\Delta Ct}$ normalizing target gene expression to *gapdh* or $2^{-\Delta\Delta Ct}$ where applicable.

AM depletion

Nonpregnant and pregnant (E8) WT mice were treated with control or clodronate liposomes (70 μl, intranasally) (Liposoma BV). Two days postdepletion (E10), mice were intranasally infected with 50 PFU IAV PR8, and lungs were harvested 1 day postinfection for quantification of viral load by MDCK plaque assay. All installations were performed under light isoflurane anesthesia.

Isolation and infection of AMs

Murine AMs were isolated from nonpregnant and pregnant mice (E10). BAL fluid was collected following five washes with 1 ml of cold PBS via a tracheal cannula. The total volume recovered after

each lavage was ~0.8 ml. Samples were spun down at a speed of 1500 rpm for 10 min, resuspended in RPMI (Gibco), 10% FBS (heat-inactivated; Wisent), 1% 200 mM L-glutamine (Gibco), 10 mM Hepes, and penicillin-streptomycin (100 U ml^{-1}; Wisent), and plated at a density of 100,000 cells per well in a 96-well plate. Cells were incubated for 1 hour, washed three times with PBS, and infected with IAV (MOI of 1) for 24 hours. RNA from AMs was extracted using the RNeasy Kit (Qiagen) according to the manufacturer's instructions.

Assessment of metabolism in AMs

AM were seeded at a density of 100,000 cells per well and infected with IAV (MOI of 1) for 1 hour. After 24 hours of incubation, cells were washed and resuspended in XF medium (nonbuffered RPMI containing 2 mM L-glutamine, 25 mM glucose, and 1 mM sodium pyruvate). Following a 1-hour incubation without CO_2 at 37°C, oxygen consumption rate of AMs was assessed using a Seahorse Xfe 96 Analyzer (Agilent Technologies). Mitochondrial stress assay was performed using the mitochondrial inhibitors oligomycin (1.5 μM), fluorocarbonyl cyanide phenylhydrazone (FCCP; 1 μM), and antimycin A and rotenone (0.5 μM) per the manufacturer's instructions. Two consecutive measurements were taken following each injection of oligomycin, FCCP, and antimycin A with rotenone. Measurements were normalized to cell number using crystal violet dye extraction. Resulting curves were generated using Wave Desktop 2.3 (Agilent Technologies).

AM adoptive transfer model

AMs from nonpregnant or pregnant mice (E10) were harvested, resuspended at a density of 5×10^4 cells per 50 μl, and intratracheally transferred into *Rag1*$^{-/-}$ mice. Two hours posttransfer, mice were infected with 50 PFU IAV PR8 intranasally. Lungs were harvested 3 days postinfection for the quantification of viral load by MDCK plaque assay.

Principal components analysis

Pearson correlation coefficients between viral *Ns1* and AMP expression as well as PCA on centered and scaled features were computed using the R "stats" library (*75*).

Administration of IL-17A blocking antibody

Nonpregnant and pregnant (E8) WT mice were administered anti–IL-17A (200 μg per mouse; #BE0173, clone 17F3, BioXCell) or anti-IgG1 (#BE0083, clone MOPC-21, BioXCell) in 200 μl of PBS intraperitoneally 2 days before and the day of IAV infection. One day after intranasal infection with 50 PFU IAV PR8, nasal cavities were harvested for AMP expression by RT-qPCR and viral quantification by MDCK plaque assay.

Administration of rIL-17A

Nonpregnant mice were administered rIL-17A (1 μg per mouse; R&D Systems, #7956-ML-025/CF) intranasally in 10 μl of PBS (5 μl per naris) 2 hours before IAV infection (50 PFU intranasally). One day postinfection, nasal cavities were harvested for *Ns1* and AMP expression by RT-qPCR.

Administration of rmBD-3

Nonpregnant mice were administered rmBD-3 (1 μg per mouse; Peprotech, #250-41-100UG) intranasally in 10 μl of PBS (5 μl per naris) 1 hour before IAV infection (50 PFU intranasally). Nasal cavities were harvested 1 day postinfection for viral *Ns1 and M1* expression by RT-qPCR.

Murine epithelial cell infection

MLE-12 cells (ATCC) were seeded at a density of 150,000 cells in 0.3 ml of MLE-12 medium [DMEM:F12 (Gibco), 2% FBS (heat-inactivated; Wisent), 1% 200 mM L-glutamine (Gibco), 1% of 100× antibiotic-antimycotic (Gibco), 2% 1 M Hepes (Gibco), and 2% of 100× insulin-transferrin-selenium (Gibco)] in a 24-well plate for 24 hours. IAV PR8 (MOI of 1) and rmBD-3 (100 μg/ml) were preincubated at 4°C for 2 hours as previously described (*76*). MLE-12 cell layer was washed once with PBS and infected with 250,000 PFU per well in 85 μl for 1 hour at 37°C. Cell layer was washed and topped with 300 μl of IAV medium [DMEM (Gibco), 0.1% BSA (Sigma-Aldrich), 1% 200 mM L-glutamine (Gibco), and 1% of 100× antibiotic-antimycotic (Gibco)] and TPCK trypsin (2 μl/ml) for 24 hours at 37°C. The following day, the supernatant was collected, and 300 μl of RLT buffer (Qiagen) was added to the cell layer in preparation for RNA extraction using the RNeasy Kit (Qiagen) according to the manufacturer's instructions.

Assessment of respiratory mechanics and airway responsiveness to MCh

Mice were administered anesthetic agents xylazine (8 to 12 mg/kg) and sodium pentobarbital (30 to 70 mg/kg) and the paralytic agent pancuronium (0.8 to 1.2 mg/kg) intraperitoneally, cannulated via tracheotomy, and connected to a mechanical ventilator (flexiVent, Scireq, Montreal, QC, Canada). Mice were challenged with increasing concentrations of aerosolized MCh (6.25, 12.5, 25, 50 mg/m of MCh) using the flexiVent on days 0, 1, and 3 postinfection while assessing respiratory mechanics (*77*). Commercial software was used to estimate the respiratory parameters, resistance, and elastance.

Statistical analysis

Statistical analysis was performed using GraphPad Prism version 10 (GraphPad Software, San Diego, CA, USA). All data are presented as mean ± SEM. Statistical differences were determined using two-way analysis of variance (ANOVA) followed by Sidak's or Tukey's multiple comparisons, one-way ANOVA followed by Holm-Šidák's multiple comparison, Kruskal-Wallis test followed by Dunn's multiple comparisons test, unpaired Student's *t* test, Mann-Whitney *U* test, or Pearson's correlation as appropriate.

Supplementary Materials

The PDF file includes:
Figs. S1 to S6
Legends for data S1 to S10

Other Supplementary Material for this manuscript includes the following:
Data S1 to S10

REFERENCES AND NOTES

1. P. R. Saunders-Hastings, D. Krewski, Reviewing the history of pandemic influenza: Understanding patterns of emergence and transmission. *Pathogens* **5**, 66 (2016).
2. M. P. Kucuk, C. E. Ozturk, N. K. Ilkaya, S. Eyupoglu, F. Ulger, A. H. Sahinoglu, Management of acute respiratory distress syndrome with H1N1 influenza virus in pregnancy: Successful mechanical ventilation and weaning with airway pressure release ventilation. *Turk. J. Anaesthesiol. Reanim.* **46**, 62–65 (2018).
3. G. Mor, P. Aldo, A. B. Alvero, The unique immunological and microbial aspects of pregnancy. *Nat. Rev. Immunol.* **17**, 469–482 (2017).

4. M. Le Gars, A. W. Kay, N. L. Bayless, N. Aziz, C. L. Dekker, G. E. Swan, M. M. Davis, C. A. Blish, Increased proinflammatory responses of monocytes and plasmacytoid dendritic cells to influenza a virus infection during pregnancy. *J. Infect Dis.* **214**, 1666–1671 (2016).
5. G. Engels, A. M. Hierweger, J. Hoffmann, R. Thieme, S. Thiele, S. Bertram, C. Dreier, P. Resa-Infante, H. Jacobsen, K. Thiele, M. Alawi, D. Indenbirken, A. Grundhoff, S. Siebels, N. Fischer, V. Stojanovska, D. Muzzio, F. Jensen, K. Karimi, H. W. Mittrucker, P. C. Arck, G. Gabriel, Pregnancy-related immune adaptation promotes the emergence of highly virulent H1N1 influenza virus strains in allogenically pregnant mice. *Cell Host Microbe* **21**, 321–333 (2017).
6. F. S. Dawood, W. Kittikraisak, A. Patel, D. Rentz Hunt, P. Suntarattiwong, M. G. Wesley, M. G. Thompson, G. Soto, S. Mundhada, C. S. Arriola, E. Azziz-Baumgartner, T. Brummer, S. Cabrera, H. H. Chang, M. Deshmukh, D. Ellison, R. Florian, O. Gonzales, K. Kurhe, S. Kaoiean, B. Rawangban, S. Lindstrom, E. Llajaruna, J. A. Mott, S. Saha, A. Prakash, S. Mohanty, C. Sinthuwattanawibool, Y. Tinoco, Incidence of influenza during pregnancy and association with pregnancy and perinatal outcomes in three middle-income countries: A multisite prospective longitudinal cohort study. *Lancet. Infect. Dis.* **21**, 97–106 (2021).
7. E. Rolland-Harris, J. Vachon, R. Kropp, J. Frood, K. Morris, L. Pelletier, R. Rodin, Hospitalization of pregnant women with pandemic A(H1N1) 2009 influenza in canada. *Epidemiol. Infect.* **140**, 1316–1327 (2012).
8. J. K. Louie, M. Acosta, D. J. Jamieson, M. A. Honein, California Pandemic (H1N1) Working Group, Pandemic working, severe H1N1 influenza in pregnant and postpartum women in California. *N. Engl. J. Med.* **362**, 27–35 (2009).
9. A. K. Malinowski, A. Noureldin, M. Othman, COVID-19 susceptibility in pregnancy: Immune/inflammatory considerations, the role of placental ACE-2 and research considerations. *Reprod. Biol.* **20**, 568–572 (2020).
10. M. Knight, K. Bunch, N. Vousden, E. Morris, N. Simpson, C. Gale, P. O'Brien, M. Quigley, P. Brocklehurst, J. J. Kurinczuk, UK Obstetric Surveillance System SARS-CoV-2 Infection in Pregnancy Collaborative Group, Characteristics and outcomes of pregnant women admitted to hospital with confirmed SARS-CoV-2 infection in UK: National population based cohort study. *BMJ* **369**, m2107 (2020).
11. D. Song, M. Prahl, S. L. Gaw, S. Narasimhan, D. Rai, A. Huang, C. Flores, C. Y. Lin, U. Jigmeddagva, A. H. B. Wu, L. Warrier, J. Levan, C. B. T. Nguyen, P. Callaway, L. Farrington, G. R. Acevedo, V. J. Gonzalez, A. Vaaben, P. Nguyen, E. Atmosfera, C. Marleau, C. Anderson, S. Misra, M. Stemmle, M. Cortes, J. McAuley, N. Metz, R. Patel, M. Nudelman, S. Abraham, J. Byrne, P. Jegatheesan, Passive and active immunity in infants born to mothers with SARS-CoV-2 infection during pregnancy: Prospective cohort study. *BMJ Open* **11**, e053036 (2021).
12. D. Sutton, K. Fuchs, M. D'Alton, D. Goffman, Universal screening for SARS-CoV-2 in women admitted for delivery. *N. Engl. J. Med.* **382**, 2163–2164 (2020).
13. E. H. Adhikari, W. Moreno, A. C. Zofkie, L. MacDonald, D. D. McIntire, R. R. J. Collins, C. Y. Spong, Pregnancy outcomes among women with and without severe acute respiratory syndrome coronavirus 2 infection. *JAMA Netw. Open* **3**, e2029256 (2020).
14. R. Medzhitov, D. S. Schneider, M. P. Soares, Disease tolerance as a defense strategy. *Science* **335**, 936–941 (2012).
15. A. Iwasaki, P. S. Pillai, Innate immunity to influenza virus infection. *Nat. Rev.Immunol.* **14**, 315–328 (2014).
16. E. Q. Littauer, E. S. Esser, O. Q. Antao, E. V. Vassilieva, R. W. Compans, I. Skountzou, H1N1 influenza virus infection results in adverse pregnancy outcomes by disrupting tissue-specific hormonal regulation. *PLOS Pathog.* **13**, e1006757 (2017).
17. G. Marcelin, J. R. Aldridge, S. Duan, H. E. Ghoneim, J. Rehg, H. Marjuki, A. C. Boon, J. A. McCullers, R. J. Webby, Fatal outcome of pandemic H1N1 2009 influenza virus infection is associated with immunopathology and impaired lung repair, not enhanced viral burden, in pregnant mice. *J. Virol.* **85**, 11208–11219 (2011).
18. C. F. Santillan Salas, S. Mehra, M. R. Pardo Crespo, Y. J. Juhn, Asthma and severity of 2009 novel H1N1 influenza: A population-based case-control study. *J. Asthma* **50**, 1069–1076 (2013).
19. C. F. Santillan Salas, S. Mehra, M. R. Pardo Crespo, Y. J. Juhn, Atopic conditions other than asthma and risk of the 2009 novel H1N1 infection in children: A case-control study. *Allergy Asthma Proc.* **34**, 459–466 (2013).
20. M. S. Vermillion, A. Nelson, L. G. Vom Steeg, J. M. Loube, W. Mitzner, S. L. Klein, Pregnancy preserves pulmonary function following influenza virus infection in C57BL/6 mice. *Am. J. Physiol. Lung Cell. Mol. Physiol.* **315**, 517–525 (2018).
21. N. S. Heaton, N. Moshkina, R. Fenouil, T. J. Gardner, S. Aguirre, P. S. Shah, N. Zhao, L. Manganaro, J. F. Hultquist, J. Noel, D. Sachs, J. Hamilton, P. E. Leon, A. Chawdury, S. Tripathi, C. Melegari, L. Campisi, R. Hai, G. Metreveli, A. V. Gamarnik, A. Garcia-Sastre, B. Greenbaum, V. Simon, A. Fernandez-Sesma, N. J. Krogan, L. C. F. Mulder, H. van Bakel, D. Tortorella, J. Taunton, P. Palese, I. Marazzi, Targeting viral proteostasis limits Influenza virus, HIV, and dengue virus infection. *Immunity* **44**, 46–58 (2016).
22. R. Gui, Q. Chen, Molecular events involved in influenza a virus-induced cell death. *Front. Microbiol.* **12**, 797789 (2021).
23. J. L. Simpson, I. Moric, P. A. B. Wark, S. L. Johnston, P. G. Gibson, Use of induced sputum for the diagnosis of influenza and infections in asthma: A comparison of diagnostic techniques. *J. Clin. Virol.* **26**, 339–346 (2003).
24. Y. J. Chang, H. Y. Kim, L. A. Albacker, N. Baumgarth, A. N. McKenzie, D. E. Smith, R. H. Dekruyff, D. T. Umetsu, Innate lymphoid cells mediate influenza-induced airway hyper-reactivity independently of adaptive immunity. *Nat. Immunol.* **12**, 631–638 (2011).
25. J. M. Gonzalez-Navajas, J. Lee, M. David, E. Raz, Immunomodulatory functions of type I interferons. *Nat. Rev. Immunol.* **12**, 125–135 (2012).
26. A. Cardani, A. Boulton, T. S. Kim, T. J. Braciale, Alveolar macrophages prevent lethal Influenza pneumonia by inhibiting infection of Type-1 alveolar epithelial Cells. *PLOS Pathog.* **13**, e1006140 (2017).
27. C. Schneider, S. P. Nobs, A. K. Heer, M. Kurrer, G. Klinke, N. van Rooijen, J. Vogel, M. Kopf, Alveolar macrophages are essential for protection from respiratory failure and associated morbidity following influenza virus infection. *PLOS Pathog.* **10**, e1004053 (2014).
28. H. E. Ghoneim, P. G. Thomas, J. A. McCullers, Depletion of alveolar macrophages during influenza infection facilitates bacterial superinfections. *J. Immunol.* **191**, 1250–1259 (2023).
29. F. Coulombe, J. Jaworska, M. Verway, F. Tzelepis, A. Massoud, J. Gillard, G. Wong, G. Kobinger, Z. Xing, C. Couture, P. Joubert, J. H. Fritz, W. S. Powell, M. Divangahi, Targeted prostaglandin E2 inhibition enhances antiviral immunity through induction of type I interferon and apoptosis in macrophages. *Immunity* **40**, 554–568 (2014).
30. E. Pernet, S. Sun, N. Sarden, S. Gona, A. Nguyen, N. Khan, M. Mawhinney, K. A. Tran, J. Chronopoulos, D. Amberkar, M. Sadeghi, A. Grant, S. Wali, R. Prevel, J. Ding, J. G. Martin, A. Thanabalasuriar, B. G. Yipp, L. B. Barreiro, M. Divangahi, Neonatal imprinting of alveolar macrophages via neutrophil-derived 12-HETE. *Nature* **614**, 530–538 (2023).
31. A. Viola, F. Munari, R. Sanchez-Rodriguez, T. Scolaro, A. Castegna, The metabolic signature of macrophage responses. *Front. Immunol.* **10**, 1462 (2019).
32. J. F. Lauzon-Joset, N. M. Scott, K. T. Mincham, P. A. Stumbles, P. G. Holt, D. H. Strickland, Pregnancy induces a steady-state shift in alveolar macrophage M1/M2 phenotype that is associated with a heightened severity of influenza virus infection: Mechanistic insight using mouse models. *J. Infect. Dis.* **219**, 1823–1831 (2019).
33. M. Divangahi, I. L. King, E. Pernet, Alveolar macrophages and type I IFN in airway homeostasis and immunity. *Trends Immunol.* **36**, 307–314 (2015).
34. T. Giri, S. Panda, J. C. Kelly, C. Pancaro, A. Palanisamy, Upregulated influenza a viral entry factors and enhanced interferon-alpha response in the nasal epithelium of pregnant rats. *Heliyon* **8**, e09407 (2022).
35. M. Palomino-Segura, I. Latino, Y. Farsakoglu, S. F. Gonzalez, Early production of IL-17A by gammadelta T cells in the trachea promotes viral clearance during influenza infection in mice. *Eur. J. Immunol.* **50**, 97–109 (2020).
36. C. Xue, M. Wen, L. Bao, H. Li, F. Li, M. Liu, Q. Lv, Y. An, X. Zhang, B. Cao, V$\gamma4^{+}\gamma\delta$T cells aggravate severe H1N1 influenza virus infection-induced acute pulmonary immunopathological injury via secreting interleukin-17A. *Front. Immunol.* **8**, 1054 (2017).
37. C. E. Sutton, S. J. Lalor, C. M. Sweeney, C. F. Brereton, E. C. Lavelle, K. H. Mills, Interleukin-1 and IL-23 induce innate IL-17 production from gammadelta T cells, amplifying Th17 responses and autoimmunity. *Immunity* **31**, 331–341 (2009).
38. N. K. Archer, N. D. Adappa, J. N. Palmer, N. A. Cohen, J. M. Harro, S. K. Lee, L. S. Miller, M. E. Shirtliff, Interleukin-17A (IL-17A) and IL-17F are critical for antimicrobial peptide production and clearance of staphylococcus aureus nasal colonization. *Infect. Immun.* **84**, 3575–3583 (2016).
39. L. Borkner, L. M. Curham, M. M. Wilk, B. Moran, K. H. G. Mills, Correction: IL-17 mediates protective immunity against nasal infection with *Bordetella pertussis* by mobilizing neutrophils, especially Siglec-F^{+} neutrophils. *Mucosal Immunol.* **14**, 1218–1219 (2021).
40. X. Wang, X. Lin, Z. Zheng, B. Lu, J. Wang, A. H. Tan, M. Zhao, J. T. Loh, S. W. Ng, Q. Chen, F. Xiao, E. Huang, K. H. Ko, Z. Huang, J. Li, K. H. Kok, G. Lu, X. Liu, K. P. Lam, W. Liu, Y. Zhang, K. Y. Yuen, T. W. Mak, L. Lu, Host-derived lipids orchestrate pulmonary gammadelta T cell response to provide early protection against influenza virus infection. *Nat. Commun.* **12**, 1914 (2021).
41. X. J. Guo, P. Dash, J. C. Crawford, E. K. Allen, A. E. Zamora, D. F. Boyd, S. Duan, R. Bajracharya, W. A. Awad, N. Apiwattanakul, P. Vogel, T. D. Kanneganti, P. G. Thomas, Lung $\gamma\delta$ T cells mediate protective responses during neonatal influenza infection that are associated with type 2 immunity. *Immunity* **49**, 531–544 (2018).
42. K. S. LeMessurier, Y. Lin, J. A. McCullers, A. E. Samarasinghe, Antimicrobial peptides alter early immune response to influenza a virus infection in C57BL/6 mice. *Antiviral Res.* **133**, 208–217 (2016).
43. K. T. Chong, R. R. Thangavel, X. Tang, Enhanced expression of murine β-defensins (MBD-1, −2,- 3, and −4) in upper and lower airway mucosa of influenza virus infected mice. *Virology* **380**, 136–143 (2008).
44. C. S. Delaveris, E. R. Webster, S. M. Banik, S. G. Boxer, C. R. Bertozzi, Membrane-tethered mucin-like polypeptides sterically inhibit binding and slow fusion kinetics of influenza a virus. *Proc. Natl. Acad. Sci. U.S.A.* **117**, 12643–12650 (2020).
45. S. M. Currie, E. Gwyer Findlay, A. J. McFarlane, P. M. Fitch, B. Bottcher, N. Colegrave, A. Paras, A. Jozwik, C. Chiu, J. Schwarze, D. J. Davidson, Cathelicidins have direct antiviral

activity against respiratory syncytial virus in vitro and protective function in vivo in mice and humans. *J. Immunol.* **196**, 2699–2710 (2016).
46. S. Tripathi, T. Tecle, A. Verma, E. Crouch, M. White, K. L. Hartshorn, The human cathelicidin LL-37 inhibits influenza A viruses through a mechanism distinct from that of surfactant protein D or defensins. *J. Gen. Virol.* **94** (Pt. 1), 40–49 (2013).
47. J. L. Sobiesk, S. Munakomi. Anatomy, Head and Neck, Nasal Cavity, in StatPearls [Treasure Island (FL): StatPearls Publishing, 2024]; https://www.ncbi.nlm.nih.gov/books/.
48. T. Dejima, K. Shibata, H. Yamada, H. Hara, Y. Iwakura, S. Naito, Y. Yoshikai, Protective role of naturally occurring interleukin-17A-producing γδ T cells in the lung at the early stage of systemic candidiasis in mice. *Infect. Immun.* **79**, 4503–4510 (2011).
49. Y. De, Q. Chen, A. P. Schmidt, G. M. Anderson, J. M. Wang, J. Wooters, J. J. Oppenheim, O. Chertov, LL-37, the neutrophil granule- and epithelial cell-derived cathelicidin, utilizes formyl peptide receptor-like 1 (FPRL1) as a receptor to chemoattract human peripheral blood neutrophils, monocytes, and T cells. *J. Exp. Med.* **192**, 1069–1074 (2000).
50. D. Yang, O. Chertov, S. N. Bykovskaia, Q. Chen, M. J. Buffo, J. Shogan, M. Anderson, J. M. Schroder, J. M. Wang, O. M. Howard, J. J. Oppenheim, β-defensins: Linking innate and adaptive immunity through dendritic and T cell CCR6. *Science* **286**, 525–528 (1999).
51. D. P. Robinson, S. L. Klein, Pregnancy and pregnancy-associated hormones alter immune responses and disease pathogenesis. *Horm. Behav.* **62**, 263–271 (2012).
52. H. Jacobsen, K. Walendy-Gnirss, N. Tekin-Bubenheim, N. M. Kouassi, I. Ben-Batalla, N. Berenbrok, M. Wolff, V. P. Dos Reis, M. Zickler, L. Scholl, A. Gries, H. Jania, A. Kloetgen, A. Dusedau, G. Pilnitz-Stolze, A. Jeridi, A. O. Yildirim, H. Fuchs, V. Gailus-Durner, C. Stoeger, M. H. de Angelis, T. Manuylova, K. Klingel, F. J. Culley, J. Behrends, S. Loges, B. Schneider, S. Krauss-Etschmann, P. Openshaw, G. Gabriel, Offspring born to influenza a virus infected pregnant mice have increased susceptibility to viral and bacterial infections in early life. *Nat. Commun.* **12**, 4957 (2021).
53. J. Jaworska, F. Coulombe, J. Downey, F. Tzelepis, K. Shalaby, I. Tattoli, J. Berube, S. Rousseau, J. G. Martin, S. E. Girardin, J. A. McCullers, M. Divangahi, NLRX1 prevents mitochondrial induced apoptosis and enhances macrophage antiviral immunity by interacting with influenza virus PB1-F2 protein. *Proc. Natl. Acad. Sci. U.S.A.* **111**, E2110–E2119 (2014).
54. M. J. Hegewald, R. O. Crapo, Respiratory physiology in pregnancy. *Clin. Chest Med.* **32**, 1–13 (2011).
55. N. Orban, E. Maughan, N. Bleach, Pregnancy-induced rhinitis. *Rhinology* **51**, 111–119 (2013).
56. T. Baudoin, T. Simunjak, N. Bacan, B. Jelavic, K. Kuna, A. Kosec, Redefining pregnancy-induced rhinitis. *Am. J. Rhinol. Allergy* **35**, 315–322 (2021).
57. H. Madanchi, M. Shoushtari, H. H. Kashani, S. Sardari, Antimicrobial peptides of the vaginal innate immunity and their role in the fight against sexually transmitted diseases. *New Microbes New Infect.* **34**, 100627 (2020).
58. C. R. Wira, M. V. Patel, M. Ghosh, L. Mukura, J. V. Fahey, Innate immunity in the human female reproductive tract: Endocrine regulation of endogenous antimicrobial protection against HIV and other sexually transmitted infections. *Am. J. Reprod. Immunol.* **65**, 196–211 (2011).
59. L. Frew, S. Makieva, A. T. McKinlay, B. J. McHugh, A. Doust, J. E. Norman, D. J. Davidson, S. J. Stock, Human cathelicidin production by the cervix. *PLOS ONE* **9**, e103434 (2014).
60. B. Puja, E. Yu, C. Kaushic, "Mucosal immunology of the female reproductive tract and its regulation by female sex hormones" in *Reproductive Immunology* (Academic Press, 2021), pp. 253–276.
61. V. C. Anipindi, P. Bagri, S. E. Dizzell, R. Jimenez-Saiz, M. Jordana, D. P. Snider, M. R. Stampfli, C. Kaushic, IL-17 production by $\gamma\delta^+$ T cells is critical for inducing T_h17 responses in the female genital tract and regulated by estradiol and microbiota. *Immunohorizons* **3**, 317–330 (2019).
62. V. L. Yarbrough, S. Winkle, M. M. Herbst-Kralovetz, Antimicrobial peptides in the female reproductive tract: A critical component of the mucosal immune barrier with physiological and clinical implications. *Hum. Reprod. Update* **21**, 353–377 (2015).
63. S. Kang, Q. Wu, J. Huang, B. Yang, C. Liang, P. Chi, C. Wu, Tissue resident memory gammadeltaT cells in murine uterus expressed high levels of IL-17 promoting the invasion of trophocytes. *Front. Immunol.* **11**, 588227 (2020).
64. G. V. Pinget, T. M. Corpuz, J. Stolp, E. L. Lousberg, K. R. Diener, S. A. Robertson, J. Sprent, K. E. Webster, The majority of murine γδ T cells at the maternal-fetal interface in pregnancy produce IL-17. *Immunol. Cell Biol.* **94**, 623–630 (2016).
65. H. Nishimura, T. Yajima, Y. Kagimoto, M. Ohata, T. Watase, K. Kishihara, F. Goshima, Y. Nishiyama, Y. Yoshikai, Intraepithelial gammadelta T cells may bridge a gap between innate immunity and acquired immunity to herpes simplex virus type 2. *J. Virol.* **78**, 4927–4930 (2004).
66. E. Rakasz, A. Mueller, S. Perlman, R. G. Lynch, γδ T cell response induced by vaginal herpes simplex 2 infection. *Immunol. Lett.* **70**, 89–93 (1999).
67. L. Monin, D. S. Ushakov, H. Arnesen, N. Bah, A. Jandke, M. Munoz-Ruiz, J. Carvalho, S. Joseph, B. C. Almeida, M. J. Green, E. Nye, S. Hatano, Y. Yoshikai, M. Curtis, H. Carlsen, U. Steinhoff, P. Boysen, A. Hayday, γδ T cells compose a developmentally regulated intrauterine population and protect against vaginal candidiasis. *Mucosal Immunol.* **13**, 969–981 (2020).
68. M. L. Alcaide, N. Strbo, L. Romero, D. L. Jones, V. J. Rodriguez, K. Arheart, O. Martinez, H. Bolivar, E. R. Podack, M. A. Fischl, Bacterial vaginosis is associated with loss of gamma delta T cells in the female reproductive tract in women in the miami women interagency HIV study (WIHS): A cross sectional study. *PLOS ONE* **11**, e0153045 (2016).
69. I. N. Hsieh, K. L. Hartshorn, The role of antimicrobial peptides in influenza virus infection and their potential as antiviral and immunomodulatory therapy. *Pharmaceuticals* **9**, 3 (2016).
70. K. Chen, T. Yoshimura, W. Gong, C. Tian, J. Huang, G. Trinchieri, J. M. Wang, Requirement of CRAMP for mouse macrophages to eliminate phagocytosed E. coli through an autophagy pathway. *J. Cell Sci.* **134**, jcs252148 (2021).
71. D. Minns, K. J. Smith, V. Alessandrini, G. Hardisty, L. Melrose, L. Jackson-Jones, A. S. MacDonald, D. J. Davidson, E. Gwyer Findlay, The neutrophil antimicrobial peptide cathelicidin promotes Th17 differentiation. *Nat. Commun.* **12**, 1285 (2021).
72. C. R. Gaush, T. F. Smith, Replication and plaque assay of influenza virus in an established line of canine kidney cells. *Appl. Microbiol.* **16**, 588–594 (1968).
73. Measuring cell fluorescence using ImageJ. https://theolb.readthedocs.io/en/latest/imaging/measuring-cell-fluorescence-using-imagej.html.
74. A. Pizzolla, T. H. O. Nguyen, J. M. Smith, A. G. Brooks, K. Kedzieska, W. R. Heath, P. C. Reading, L. M. Wakim, Resident memory $CD8^+$ T cells in the upper respiratory tract prevent pulmonary influenza virus infection. *Sci. Immunol.* **2**, 12 (2017).
75. Team, R.C. R: A Language and Environment for Statistical Computing. R Foundation for Statistical Computing 2023; https://R-project.org/.
76. Y. Jiang, D. Yang, W. Li, B. Wang, Z. Jiang, M. Li, Antiviral activity of recombinant mouse β-defensin 3 against influenza A virus in vitro and in vivo. *Antivir. Chem. Chemother.* **22**, 255–262 (2012).
77. T. K. McGovern, A. Robichaud, L. Fereydoonzad, T. F. Schuessler, J. G. Martin, Evaluation of respiratory system mechanics in mice using the forced oscillation technique. *J. Vis. Exp.* **75**, e50172 (2013).

Acknowledgments: We would like to acknowledge the Histopathology platform at the RI-MUHC, S. Joy, B. Thurairajah, and E. Ahmed for the assistance with tissue processing and histology and immunohistochemistry staining, quantification of histology, flow cytometry for $\gamma\delta^+$ T cells, and PCA, respectively. Graphical models were designed using https://biorender.com/. **Funding:** The study was funded by grants from the Richard and Edith Strauss Foundation and the Canadian Institute of Health Research (CIHR) Project Grant PJT-186275 (held by J.G.M. and M.D.). M.D. holds a Fonds de Recherche du Québec–Santé Award and the Strauss Chair in Respiratory Diseases and is a fellow of the Royal Society of Canada. J.C. was supported by studentships from the Research Institute of the McGill University Health Center.
Author contributions: Conceptualization: J.C., M.D., and J.G.M.; methodology: J.C., M.D., and J.G.M.; validation: J.C., M.D., and J.G.M.; investigation: J.C., E.P., K.A.T., T.K.M., A.M., O.T., K.M., and M.D.; formal analysis: J.C., E.P., K.A.T., T.K.M., A.M., O.T., S.W., and K.M.; writing—original draft: J.C. and J.G.M.; writing—review and editing: J.C., E.P., M.D., and J.G.M.; project administration: J.C., M.D., and J.G.M.; supervision: M.D. and J.G.M.; resources: M.D. and J.G.M.; funding acquisition: M.D. and J.G.M. **Competing interests:** The authors declare that they have no competing interests. **Data and materials availability:** All data needed to evaluate the conclusions in the paper are present in the paper and/or the Supplementary Materials.

Submitted 16 February 2024
Accepted 23 August 2024
Published 27 September 2024
10.1126/sciadv.ado7087